1   Referee comments are given in *Blue*.

2   Response to comments are given in Black.

3   In the manuscript <mark>highlighted</mark> text is the added text and ~~red crossed out~~ text is deleted text.

4   **Response to Referee 1**

5   We thank the reviewer for the comments on our manuscript. Please see below for our
6   responses.

7   *Comment 1 – In lines 55-62 authors talk about different works on the A-band and mentioning*
8   *Galatry retrievals. However, for some reason the work of Drouin et al (JQSRT 2016) was not*
9   *mentioned although it also employed the SDV profile.*
10
11   We acknowledge that the work by Drouin et al. (2017) uses a SDV profile when fitting the A-
12   band and have included it in the introduction of when discussing the line shape work done with
13   the O_2 A-band.
14
15   We have added the following on lines 80-82: "When fitting cavity ring-down spectra of the O_2
16   A-band, Drouin et al. (2017) found it necessary to use a speed-dependence Voigt line shape,
17   which takes into account different speeds at the time of collision (Shannon et al., 1986), with
18   line mixing to properly fit the discrete spectral lines of the O_2 A-band."
19
20   *Comment 2 – The authors may want to mention that the HITRAN2016 parameters are very*
21   *similar to those in HITRAN2012 in this particular band and the only change are improved line*
22   *positions from Yu et J. Chem. Phys. 141 (2014) 174302. doi:10.1063/1.4900510.*
23
24   We acknowledge that this should be included in the introductory section about the discrete O_2
25   1.27 μm band since it is the latest version of the spectroscopic parameters used for this band.
26
27   We have added the following on lines 64-66: "Spectroscopic parameters for the discrete
28   spectral lines of the O_2 1.27 μm band from HITRAN 2016 (Gordon et al., 2017) are very similar
29   to HITRAN 2012 except that HITRAN2016 includes improved line positions reported by Yu et al.
30   (2014)."
31
32   *Comment 3 – It is interesting that the authors do mention the line-mixing with respect to the*
33   *Aband and CO2 bands but did not say about this effect in 1.27 micron band that they*
34   *investigated. It is also not mentioned as potential source of remaining residuals in lines*
35   *293-303. It would be interesting to see some discussion about this.*

36   We have added a discussion about line mixing and how it impacts some of the retrieved
37   spectroscopic parameters as well as the remaining residuals seen when fitting the lab spectra.

38 We have added the following on lines 359-367: "This can be explained by the fact that line mixing,
39 which is shown to be important for the O_2 A-band, was not considered when fitting the cavity-ringdown
40 spectra. Neglecting line mixing usually produces an asymmetric residual in the discrete lines as well as a
41 broad residual feature associated with the fact that collisions are transferring intensity from one part of
42 the spectrum to another. By fitting a set of Legendre polynomials for CIA we could simultaneously be
43 fitting the broader band feature associated with line mixing while the retrieved pressure shifts, and
44 speed-dependent pressure shifts could be compensating for the asymmetric structure one would see in
45 the discrete lines when neglecting line mixing. The remaining structure, as seen in Figure 1c, could be
46 due to neglecting line mixing especially in the Q-branch where the spacing between spectral lines is
47 small (in comparison to the P and R branches) and line mixing is most likely prevalent."

48 *Comment 4* – Talking about the sources of the residuals and its potential relation to Dicke
49 narrowing it would be interesting what authors think about conclusions of the Torun group
50 (Domyslawska et al papers in JQSRT 2014-2016), that for the electronic transitions of
51 O2 speed-dependence should have much larger effect than Dicke narrowing.

52 To address this comment we have added the following discussion on lines 371-383:
53 "Domysławska et al. (2016) recommend using the qSDV to model the line shape of O_2 based on
54 multiple line shape studies of the O_2 B-band. In these studies, a multi-spectrum fit to low
55 pressure (0.27-5.87 kPa) cavity-ring down spectra was preformed testing multiple line shapes
56 that took speed-dependence and Dicke narrowing into account both separately and
57 simultaneously. They found that the line shapes that only used Dicke narrowing were not good
58 enough to model the line shape of the O_2 B-band lines, but a line shape that included either
59 speed-dependence or both speed-dependence and Dicke narrowing produced similar quality
60 fits, ultimately concluding that speed-dependence has a larger effect than Dicke narrowing. It
61 was noted in the study by Wójtewicz et al., (2014) that both Dicke narrowing and speed-
62 dependent effects might simultaneously play an important role in modeling the line shape of
63 the O_2 B-band lines. However, the speed-dependent and Dicke narrowing parameters are highly
64 correlated at low pressures. To reduce the correlation requires either a multi-spectrum fit of
65 spectra at low pressures with high enough signal to nosie ratio or spectra that cover a wide
66 range of pressure (Wójtewicz et al., 2014). So, by combining the high-pressure spectra used in
67 this study with low pressure spectra in a multipspectrum fit both the speed-dependence and
68 Dicke narrowing parameters could be retrieved."

69 *Comment 5* – Spectral shifts in the 1.27 micron band had always been very hard to measure.
70 See for instance discussion in Hill et al, J. Mol. Spectrosc. 221 (2003) 286–287.
71 doi:10.1016/S0022-2852(03)00227-3 and Newman, et al, J. Chem. Phys. 110 (1999)
72 10749. doi:10.1063/1.479018.
73
74 The authors may want to mention this. Continuing the topic of shifts it is well known that
75 while the widths in P and R branches for same rotational quanta should be very similar

76 the shifts should be assymetric. Therefore I would suggest to plot these separately
77 or using running number m, where m=-J for P lines and J+1 for R. The authors may
78 also want to use the upper state rotational quanta because they are not split into spin
79 components.

80 We have added the following on lines 356-359, to address this comment: "Accurate
81 measurements of the pressure shifts in the 1.27 µm band have been hard to obtain as shown in
82 Newman et al. (1999) and Hill et al., (2003). While the retrieved pressure shifts show a
83 dependence on quantum number m (Figure 3c) as one would expect, this dependence is not as
84 strong as the m dependence of the Lorentz widths (Figure 3b)."

85 We have also replotted Figures 3 and 4 to show the retrieved parameters as a function of m.

86 *Comment 6 -* Does one need to account for airglow when analysing the 1.27 TCCON spectra?
87 See Sun et al (https://doi.org/10.1029/2018GL077823) for instance, regarding significance
88 of airglow in oxygen's 1.27 micron band at the top of atmosphere.

89 Since TCCON spectra are recorded by viewing the sun directly, airglow emission is negligible
90 since the signal from the sun is much more intense than airglow.

91 We have added the following on lines 220-221: "Airglow is not considered when fitting the 1.27
92 µm band since the spectrometer views the sun directly, and airglow is overwhelmed by such a
93 bright source."

94 **Response to Referee 2**

95 We thank the reviewer for the comments on our manuscript. Please see below for our response
96 to the comments.

97 *Comment 1 -* The paper is very theoretical. Line 92 starts with: to take speed dependence into
98 account … Here it would be nice to explain what is meant by speed dependence. It should be
99 mentioned that the assumed basis for the Lorentz portion of the Voigt profile is, that for all
100 collisions between the molecules the statistical average velocity is taken. However, in reality
101 this is not true, the molecules have a distribution of speeds, which requires the qSDV.
102
103 To address this we have added the following:
104
105 Lines 104-105: "The Voigt line shape is the convolution of the Lorentz and the Gaussian profiles,
106 which model pressure and doppler broadening of the spectral line respectively."
107
108 Lines 112-113: "The Voigt line shape assumes that pressure broadening is accurately
109 represented by a Lorentz profile calculated for the stastical average velocity at the time of
110 collission."
111

112   Lines 115-118: "The speed-dependent Voigt line shape refines the pressure broadening
113   component of the Voigt by calculating multiple Lorentz profiles for different speeds at the time
114   of collision. The final contribution from pressure broadening to the speed-dependent Voigt is
115   the weighted sum of Lorentz profiles (weighted by the Maxwell-Boltzmann speed-distribution)
116   calculated for different speeds at the time of collision."

117

118   *Comment 2* - The same holds for the Dicke narrowing, mentioned in line 59. What is the Dicke
119   narrowing? It should be mentioned that when the mean free path of an atom is much smaller
120   than the wavelength of the radiative transition, the atom changes velocity and direction many
121   times during the emission or absorption of a photon. This causes an averaging over different
122   Doppler states and results in an atomic linewidth that is narrower than the Doppler width (I
123   have taken this from Wikipedia).

124

125   To address this comment we have added the following:

126

127   Lines 71-74: "Dicke narrowing occurs when the motion of the molecule is diffusive due to
128   collisions changing the velocity and direction of the molecule during the time that it is excited.
129   This diffusive motion is taken into account by averaging over many different Doppler states
130   resulting in a line width that is narrower than the Doppler width (Dicke, 1953)."

131

132   *Comment 3* - The O2 concentration in the atmosphere is very stable and well known. I would be
133   interested to see the difference between the known O2 concentration and the O2 from the
134   TCCON spectra as a function of the SZA. These results are somehow hidden in the paper (Figure
135   6), but since the qSDV is applied to CO2 and O2 it would be good to see where the differences
136   mentioned (0.004) are coming from, from CO2 or O2.

137

138   To address this comment we have added another figure (Figure 7) which shows XAIR calculated
139   using the column of O_2 retrieved with the Voigt and the qSDV. Ideally XAIR should be 1 since the
140   column of O_2 is being used as a proxy for the dry column of air when calculating XCO_2. However
141   as shown in Figure 7 it is not. When using a Voigt lie shape to retrieve the O_2 column, XAIR is 2%
142   lower than it should be (at the smallest SZA) and has an airmass dependence that decreases as
143   SZA increases (so the retrieved O_2 column increases as SZA increases). By using the qSDV to
144   retrieve the O_2 column, less O_2 is retrieved which results in the O_2 column decreasing by 0.8% at
145   the smallest SZA and up to 1.8% at the highest SZA as shown in Figure 6. Thus when the qSDV is
146   used to retrieve O_2 XAIR is closer to 1.The airmass dependence of XAIR changes when O_2 is
147   retrieved with the qSDV, causing XAIR to now increase as the airmass increases. The airmass
148   dependence of the O_2 column is thus similar to the airmass dependence of the CO_2 column, so
149   when calculating XCO_2 with the column of O_2 retrieved using the qSDV, the airmass dependence
150   of XCO_2 is minimized as shown in the new Figure 8.

151

152   We have added the following on lines 254-261: "Figure 7 shows XAIR from Park Falls on June
153   18, 2013. XAIR is the column of air (determined using surface pressure recorded at the site)
154   divided by the column of O_2 retrieved from the spectra and multiplied by 0.2095, which is the
155   dry air mole fraction of O_2 in Earth's atmosphere. Ideally XAIR should be 1 but when using O_2

156 retrieved with a Voigt line shape (red points) it is closer to 0.98 near noon (small SZA) and lower
157 near the start and end of the day (large SZA). When using O_2 retrieved with the qSDV, XAIR is
158 closer to 0.988 near noon and a bit higher near the start and end of the day. This means the O_2
159 column, retrieved with the qSDV, decreases as a function of SZA, while previously the column
160 increased as a function of SZA when the Voigt line shape is used."

162 We address the comment about the 0.004 change in comment 4.

164 *Comment 4* - I found it a bit disappointing that the airmass dependance is now + 0.004 instead
165 of - 0.013. This is a large reduction, but the results show that still something is wrong in the
166 measurements/retrieval. The authors might discuss this in more detail. See above at 3.

168 The positive bias that now exists with the new spectroscopy is because the retrieved columns
169 of CO_2 have increased when retrieved using the qSDV with line mixing while the retrieved
170 columns of O_2 have decreased with the qSDV. This combination of an increase in the CO_2
171 column with a decrease in the O_2 column results in an increase in XCO_2. The decrease in
172 retrieved O_2 column is good as noted in comment 3 but still needs to decrease further to match
173 the column of dry air calculated from surface pressure measured at the TCCON stations. So if
174 the retrieved O_2 column decreased further the positive bias between TCCON and the aircraft
175 measurements would increase. This means that the retrieved columns of CO_2 are too high but
176 for now compensate for the fact that the retrieved O_2 columns are still larger than they should
177 be.

179 We have added the following to discuss this point on lines 319-324: "This increase in the slope
180 can be explained by an increase in the retrieved column of CO_2 when using the qSDV with line
181 mixing as shown in Mendonca et al. (2016) as well as combined with a decrease in the retrieved
182 O_2 column due to using the qSDV. As discussed previously (section 5) the decrease in the
183 retrieved O_2 column is an improvement but the expected column of O_2 is still approximately
184 1.2% higher (at the smallest SZA) than it should be. Therefore, the retrieved column of CO_2 is
185 higher than it should be, and the slope would be greater if the retrieved column of O_2 was 1.2%
186 lower."

188 *Comment 5* - For me the fact that the airmass dependence is nearly gone when applying qSDV
189 (Figure 8) very important. This should be more highlighted as main result. Figure 8 c and d look
190 very similar. For me an airmass correction is not necessary, or is this a mistake in the panels?

192 Figures 8c and 8d are now Figures 10c and 10d. Figures 10c and 10d do look very similar but
193 there is still an airmass dependence given by the fact that the correction term is not 0. It is now
194 -0.0012, which is smaller than with a Voigt, but we still need to apply the correction to the data
195 to account for this small airmass dependence. Since the airmass dependence has been
196 significantly decreased Figures 10c and d look similar but are not the same.

198 *Comment 6* - May be a Figure showing XCO2/O2 as a function of SZA for i) XCO2/O2, ii)
199 XCO2(sQDV)/O2 ii) XCO2/O2(sQDV), iii) XCO2 (qSDV)/O2(qSDV) would be interesting to see

200 where the improvement is coming from. For me a few other Figures of 1-5 could be deleted or
201 put in the supplement.
202
203 We have added Figure 8 to show how the changes to the retrieved CO_2 or O_2 affect their
204 airmass dependence. Figure 8 shows that the improvement of the retrieved column of O_2 has a
205 greater impact than the improvements made to the retrieval of CO_2. However, the
206 improvement made to the retrieval of CO_2 are more critical at large SZA because it makes the
207 airmass dependence of the column of CO_2 for large SZA consistent with that for small SZA,
208 allowing the SZA restriction on measurements at large SZA to be removed.
209
210 We have added the following lines 265-278: "Figure 8 is XCO_2 calculated for four different
211 combinations pertaining to the two CO_2 column retrievals and the O_2 column retrievals. The
212 CO_2 columns were retrieved with either a Voigt line shape (the standard GGG2014 approach) or
213 the qSDV with line mixing as done in Mendonca et al. (2016) while the O_2 columns were
214 retrieved with either a Voigt (the standard GGG2014 approach) or the new qSDV approach
215 developed here. Figure 8 shows a spurious symmetric component to XCO_2 when the total
216 column of O_2 is retrieved with the Voigt line shape, regardless of line shape used to retrieve
217 CO_2. When the qSDV is used to retrieve total columns of O_2, the symmetric component of XCO_2
218 is diminished regardless of line shape used to retrieve CO_2. This is because the airmass
219 dependence of the column of O_2 retrieved using the qSDV is more consistent with the airmass
220 dependence of the column of CO_2 (for both line shapes used to retrieve CO_2). Mendonca et al.
221 (2016) showed that using the qSDV with line mixing results in better fits to the CO_2 windows
222 and impacts the airmass dependence of the retrieved column of CO_2. When using a Voigt line
223 shape the retrieved column amount of CO_2 decreases as airmass increases until the airmass is
224 large (SZA of about 82°) at which point the retrieved column of CO_2 increases as the airmass
225 increases, changing the shape of the airmass dependence of the CO_2 column. When the qSDV
226 with line mixing is used, the retrieved column of CO_2 decreases as a function of airmass (up
227 until the sun is above the horizon)."
228
229 It is important that the Figures 1-5 remain since they show that the retrieved spectroscopic
230 parameters have a dependence on quantum number m which has been shown to be the case in
231 other studies of the discrete lines of the O_2 1.27 µm electronic transitions.
232
233 *Comment 7 –* The main part of the paper deals with the speed-dependent Voigt line shape. I
234 would suggest to include this in the title, may by: Improving the Retrieval of XCO2 from Total
235 Carbon Column Network Solar Spectra by inclusion of the speed-dependent Voigt line shape.
236
237 Changed the title to: "Using a Speed-Dependent Voigt Line Shape to Retrieve O_2 from Total
238 Carbon Column Observing Network Solar Spectra to Improve Measurements of XCO_2"
239
240 *Comment 8 -* In the conclusions the authors write: Using cavity ring-down spectra measured in
241 the lab, we have shown that the Voigt line shape is insufficient to 290 model the line shape of
242 O2 for the 1.27 µm band, ... As far as I see, the improvement might also results because the
243 qSDV is applied also the CO2.

244

245 The improvement made to the retrieval of O_2 has had an impact on the airmass dependence of

246 XCO_2 at all SZA while the improvements to the retrieval of CO_2 has mainly impacted the airmass

247 dependence at high SZA. As shown in Figure 8 using the O_2 columns retrieved with the qSDV

248 decreased the airmass dependence of XCO_2 regardless of the line shape used to retrieve the

249 CO_2 columns. However, improvements made to the CO_2 retrievals results in better

250 measurements of XCO_2 at high SZA. See comment 6 for discussion on this.

251

252 **Additional Changes to the Manuscript**

253 In the introduction, added a reference to Wallace and Livingston (1990) since they were the

254 first to measure O_2 from this band.

255 Added references for the TCCON data versions and GGG2014 spectral line list versions.

256 Changed Figures 1b, 1c, 2b, and 2c as the scale on the y-axis was wrong since the units for the

257 residuals were not consistent with the units used in Figures 1a and 2a.

258 Corrected x-axis of Figure 13.

259 Some minor typographical and phrasing corrections were made.

260

261

262

263

264

265

266

267

268

269

Using a Speed-Dependent Voigt Line Shape to Retrieve O_2 from Total Carbon Column Observing Network Solar Spectra to Improve Measurements of XCO_2 ~~Improving the Retrieval of XCO_2 from Total Carbon Column Network Solar Spectra~~

Authors: Joseph Mendonca[1], Kimberly Strong[1], Debra Wunch[1], Geoffrey C. Toon[2], David A. Long[3], Joseph T. Hodges[3], Vincent T. Sironneau[3], and Jonathan E. Franklin[4].

1. Department of Physics, University of Toronto, Toronto, ON, Canada

2. Jet Propulsion Laboratory, Pasadena, CA, USA

3. National Institute of Standards and Technology, Gaithersburg, MD, USA

4. Harvard John A. Paulson School of Engineering and Applied Sciences, Cambridge, MA, USA

Correspondence to: Joseph Mendonca (joseph.mendonca@utoronto.ca)

Abstract. High-resolution, laboratory, absorption spectra of the $a^1\Delta_g \leftarrow X^3\Sigma_g^-$ oxygen(O_2) band measured using cavity ring-down spectroscopy were fitted using the Voigt and speed-dependent Voigt line shapes. We found that the speed-dependent Voigt line shape was better able to model the measured absorption coefficients than the Voigt line shape. We used these line shape models to calculate absorption coefficients to retrieve atmospheric ~~T~~total columns abundances of O_2 ~~were retrieved~~ from ground-based ~~high resolution absorption~~ spectra from four Fourier transform spectrometers that are apart of the Total Carbon Column Observing Network (TCCON) ~~sites using both Voigt and speed-dependent Voigt line shapes to calculate absorption coefficients. A l~~Lower O_2 ~~concentration~~ total columns ~~was~~ were retrieved with the speed-dependent Voigt line shape, ~~with~~ and the difference between the total columns retrieved using the Voigt and speed-dependent Voigt line shapes ~~increasing~~ increased as a function of solar zenith angle. Previous work has shown that carbon dioxide (CO_2) total columns ~~were also retrieved from the same spectra using a Voigt line shape and~~ are better retrieved using a speed-dependent Voigt line shape with line mixing. The column-averaged dry-air mole fraction of CO_2 (XCO_2) was calculated using the ratio between the columns of CO_2 and O_2 ~~columns~~ retrieved (from the same spectra) with both line shapes from measurements made over a one-year period at the four sites. ~~and compared.~~ The inclusion of speed dependence in the O_2 retrievals significantly reduces the airmass dependence of XCO_2. ~~The TCCON empirical airmass correction factor for XCO_2 derived from a year of measurements from TCCON sites at Darwin, Lamont, and Park Falls for XCO_2 improved from -0.0071±0.0057 to -0.0012±0.0054 when speed dependence was included. XCO_2 retrieved with the Voigt and speed-dependent Voigt line shapes was compared to aircraft profiles measured at 13 TCCON sites. T~~ and the bias between the TCCON measurements and ~~the~~ calibrated integrated aircraft profile measurements was reduced from ~~0.9897±0.0005~~ 1% to ~~1.0041±0.0005~~ 0.4%. ~~for XCO_2 retrieved with the Voigt and speed-dependent Voigt line shapes respectively.~~ These results suggest that speed dependence should be included in the forward model when fitting near-infrared CO_2 and O_2 spectra to improve the accuracy of XCO_2 measurements.

1. Introduction

Accurate remote sensing of greenhouse gases (GHGs), such as CO_2, in Earth's atmosphere is important for studying the carbon cycle ~~in order~~ to better understand and predict climate change. The absorption of solar radiation by O_2 in the Earth's atmosphere is important because it can be used to study the properties of clouds and aerosols, and to determine vertical profiles of temperature and surface pressure. Wallace and Livingston (1990) were the first to retrieve total columns of O_2 from some of the discrete lines of the $a^1\Delta_g \leftarrow X^3\Sigma_g^-$ band of O_2 centered at 1.27 µm (which will be referred to bellow as the 1.27 µm band) using atmospheric solar absorption spectra from the Kitt Peak observatory. Mlawer et al. (1998) recorded solar absorption spectra in the near-infrared (NIR) region to study collision-induced absorption (CIA) in the $a^1\Delta_g \leftarrow X^3\Sigma_g^-$ band ~~of O_2 centered at 1.27 µm (which will be referred to as the 1.27 µm band)~~ as well as two other O_2 bands. The spectra were compared to a line-by-line radiative transfer model and the differences between the measured and calculated spectra showed the need for better absorption coefficients in order to accurately model the 1.27 µm band (Mlawer et al., 1998). Subsequently, spectroscopic parameters needed to calculate the absorption coefficients from discrete transitions of the 1.27 µm band were measured in multiple studies (Cheah et al., 2000; Newman et al., 1999, 2000; Smith and Newnham, 2000), as was collision-induced absorption (CIA) (Maté et al., 1999; Smith and Newnham, 2000), while Smith et al. (2001) validated the work done in Smith and Newnham (2000) using solar absorption spectra.

The 1.27 µm band is of particular importance to the Total Carbon Column Observing Network (TCCON) (Wunch et al., 2011). TCCON is a ground-based remote sensing network that makes accurate and precise measurements of GHGs for satellite validation and carbon cycle studies. Using the O_2 column retrieved from solar absorption spectra, the column-averaged dry-air mole fraction of CO_2 (XCO$_2$) has been shown to provide better precision than using the surface pressure to calculate XCO$_2$ (Yang et al., 2002) ~~(Washenfelder et al., 2006)~~. The O_2 column is retrieved from the 1.27 µm band because of its close proximity to the spectral lines used to retrieve CO_2, thereby reducing the impact of solar tracker mis-pointing and an imperfect instrument line shape (ILS) (Washenfelder et al., 2006). To improve the retrievals of O_2 from the 1.27 µm band, Washenfelder et al. (2006) found that adjusting the spectroscopic parameters in HITRAN 2004 (Rothman et al., 2005) decreased the airmass and temperature dependence of the O_2 column. These revised spectroscopic parameters were included in HITRAN 2008 (Rothman et al., 2009). Atmospheric solar absorption measurements from this band made at the Park Falls TCCON site by Washenfelder et al. (2006) were the first measurements to observe the electric-quadrupole transitions (Gordon et al., 2010). Leshchishina et al. (2011, 2010) subsequently used cavity-ring-down spectra to retrieve spectroscopic parameters for the 1.27 µm band using a Voigt spectral line shape and these parameters were included in HITRAN 2012 (Rothman et al., 2013). Spectroscopic parameters for the discrete spectral lines of the O_2 1.27 µm band from HITRAN 2016 (Gordon et al., 2017) are very similar to HITRAN 2012 except that HITRAN2016 includes improved line positions reported by Yu et al. (2014).

Extensive spectral line shape studies have been performed for the O_2 A-band, which is centered at 762 nm and used by the Greenhouse Gases Observing Satellite (GOSAT) (Yokota et al., 2009) and the Orbiting Carbon ~~Observing~~

338 Observatory-2 (OCO-2) satellite (Crisp et al., 2004) to determine surface pressure. ~~These studies~~ Studies have
339 ~~showed~~ shown that the Voigt line shape ~~was~~ is inadequate to describe the spectral line shape of the discrete O_2 lines
340 in the A-band~~;~~. Dicke narrowing occurs when the motion of the molecule is diffusive due to collisions changing the
341 velocity and direction of the molecule during the time that it is excited. This diffusive motion is taken into account
342 by averaging over many different Doppler states resulting in a line width that is narrower than the Doppler width
343 (Dicke, 1953). ~~The need to take into account Dicke narrowing was shown in~~ Long et al. (2010) and Predoi-Cross et
344 al. (2008) found it necessary to use a spectral Line shape model that accounted for Dicke narrowing when fitting the
345 discrete lines of the O_2 A-band. ~~and~~ Line mixing, which occurs when collisions transfer intensity from one part of
346 the spectral band to another (Lévy et al., 1992), was shown to be prevalent in multiple studies (Predoi-Cross et al.,
347 2008; Tran et al., 2006; Tran and Hartmann, 2008). Tran and Hartmann (2008) showed that including line mixing
348 when calculating the O_2 A-band absorption coefficients reduced the airmass dependence of the O_2 column retrieved
349 from TCCON spectra. When fitting cavity ring-down spectra of the O_2 A-band, Drouin et al. (2017) found it
350 necessary to use a speed-dependence Voigt line shape, which takes into account different speeds at the time of
351 collision (Shannon et al., 1986), with line mixing to properly fit the discrete spectral lines of the O_2 A-band.

352 The need to include non-Voigt effects when calculating absorption coefficients for the O_2 1.27 µm band was first
353 shown in Hartmann et al. (2013) and Lamouroux et al. (2014). In Hartmann et al. (2013) and Lamouroux et al.
354 (2014), Lorentzian widths were calculated using the re-quantized classical molecular-dynamics simulations
355 (rCMDSs) and used to fit cavity-ring-down spectra with a Voigt line shape for some isolated transitions in the O_2
356 1.27 µm band. The studies concluded that a Voigt line shape is insufficient for modeling the spectral lines of the O_2
357 1.27 µm band and that effects such as speed dependence and Dicke narrowing should be included in the line shape
358 calculation.

359 In this study, air-broadened laboratory cavity-ring-down spectra of the O_2 1.27 µm band were fitted using a spectral
360 line shape that takes into account speed dependence. The ~~corresponding~~ derived spectroscopic parameters for the
361 speed-dependent Voigt line shape were used to calculate absorption coefficients when fitting high-resolution solar
362 absorption spectra. Using these new O_2 total columns, and the simultaneously measured ~~were combined with~~ CO_2
363 total columns, ~~from~~ using the updated line shape model described by Mendonca et al. (2016), to calculate XCO_2 and
364 compared these results with XCO_2 retrieved using a Voigt line shape. Section 2 details the formulas used to
365 calculate absorption coefficients using different spectral line shapes. In Section 3, we describe the retrieval of
366 spectroscopic parameters from three air-broadened cavity-ring-down spectra fitted with a speed-dependent Voigt
367 line shape. For Section 4, the speed-dependent line shape along with the retrieved spectroscopic parameters is used
368 to fit solar absorption spectra from four TCCON sites and retrieve total columns of O_2, which is compared to O_2
369 retrieved using a Voigt line shape. In Section 5, we investigate the change in the airmass dependence of XCO_2 with
370 the new O_2 ~~parameters~~ retrievals. In Section 6, we discuss our results and their implications for remote sensing of
371 greenhouse gases.

372 **2. Absorption Coefficient Calculations**

2.1 Voigt Line Shape

The Voigt line shape is the convolution of the Lorentz and the Gaussian ~~Doppler line shapes~~ profiles, which model pressure and Doppler broadening of the spectral line respectively. The corresponding absorption coefficient, k, at a given wavenumber v becomes :

$$k(v) = N \sum_j S_j \left(\frac{1}{\gamma_{D_j}}\right)\left(\frac{\ln(2)}{\pi}\right)^{1/2} \left(Re[c(v, x_j, y_j)]\right) \tag{1}$$

where N is the number density, S_j is the line intensity of spectral line j, γ_{D_j} is the Doppler half-width (HWHM), c is the complex error function, and

$$x_j = \frac{\left(v - v_j^o - P\delta_j^o\right)}{\gamma_{D_j}}(\ln(2))^{1/2}, \; y_j = \frac{\gamma_{L_j}}{\gamma_{D_j}}(\ln(2))^{1/2} . \tag{2}$$

Here, v_j^o is the position of the spectral line j, P is the pressure, and δ_j^o is the pressure-shift coefficient. The Lorentz half-width, γ_{L_j}, is calculated using:

$$\gamma_{L_j}(T) = P \, \gamma_{L_j}^o \left(\frac{296}{T}\right)^n \tag{3}$$

where $\gamma_{L_j}^o$ is the air-broadened Lorentz half-width coefficient (at reference temperature 296 K) and n is the exponent of temperature dependence. The Voigt line shape assumes that pressure broadening is accurately represented by a Lorentz profile calculated for the stastical average velocity at the time of collission.

2.2 Speed-Dependent Voigt Line Shape

The speed-dependent Voigt line shape refines the pressure broadening component of the Voigt by calculating multiple Lorentz profiles for different speeds at the time of collision. The final contribution from pressure broadening to the speed-dependent Voigt is the weighted sum of Lorentz profiles (weighted by the Maxwell-Boltzmann speed-distribution) calculated for different speeds at the time of collision. ~~To take speed dependence into account, we use t~~The speed-dependent Voigt line shape (Ciuryło, 1998) with the quadratic representation of the Lorentz width and pressure shift (Rohart et al., 1994) is:

$$k(v) = N \left(\frac{2}{\pi^{\frac{3}{2}}}\right) \sum_j S_j \int_{-\infty}^{\infty} e^{-V^2} V \left(tan^{-1}\left[\frac{x_j - Ba_{\delta_j}(~~(V)~~V^2 - 1.5) + V}{y_j(1 + a_{\gamma_{L_j}}(~~(V)~~V^2 - 1.5))}\right]\right) dV \tag{4}$$

where $a_{\gamma_{L_j}}$ is the speed-dependent Lorentz width parameter (unitless) for line j, a_{δ_j} is the speed- dependent pressure-shift parameter (unitless), B is $\frac{(\ln(2))^{1/2}}{\gamma_{D_j}}$, V is the ratio of the absorbing molecule's speed to the most probable speed of the absorbing molecule, and all other variables are defined before.

11

3. Fitting Laboratory Spectra

O_2, unlike CO_2 and CH_4, cannot produce an electric dipole moment and therefore should not be infrared active. However, O_2 has two unpaired electrons in the ground state that produce a magnetic dipole moment. Due to the unpaired electrons in the ground state ($X^3\Sigma_g^-$) the rotational state (N) is split into three components which are given by $J = N$-1, $J = N$, and $J = N$+1, while in the upper state ($a^1\Delta_g$), $J = N$. When labeling a transition, the following nomenclature is used $\Delta N(N'')\Delta J(J'')$ (Leshchishina et al., 2010), where ΔN is the difference between N' in the upper state and N'' in the lower state, ΔJ is the difference between J' in the upper state and J'' in the lower state. The magnetic transitions of $a^1\Delta_g \leftarrow X^3\Sigma_g^-$ allow for ΔJ=0, ±1. This leads to 9 branches observed: P(N'')Q(J''), R(N'')Q(J''), and Q(N'')Q(J''), for ΔJ=0, O(N'')P(J''), P(N'')P(J''), and Q(N'')P(J''), for ΔJ=-1, and S(N'')R(J''), R(N'')R(J''), and Q(N'')R(J''), for ΔJ=1.

Absorption coefficients for three room temperature air-broadened (NIST Standard reference materal® 2659a containing 79.28 % N_2, 20.720(43) % O_2, 0.0029 % Ar, 0.00015 % H_2O, and 0.001 % other compounds) spectra were measured at the National Institute of Standards and Technology (NIST) using the frequency-stabilized cavity-ring-down spectroscopy (FS-CRDS)) technique (Hodges et al., 2004; Hodges, 2005). The absorption spectra were acquired at pressures of 131 kPa, 99.3 kPa, and 66.9 kPa, at temperatures of 296.28 K, 296.34 K, and 296.30 K respectively. Figure 1a shows the three measured absorption spectra. A more detailed discussion of the present FS-CRDS spectrometer can be found in Lin et al. (2015).

The spectra were fitted individually using a Voigt line shape (Eq. 1), with S_j, $\gamma_{L_j}^o$, and δ_j^o for the main isotope of the magnetic dipole lines of the O_2 1.27 µm band for lines with an intensity greater than 7.0×10^{-28} cm^{-1}/(molecule cm^{-2}). The spectroscopic parameters measured in Leshchishina et al. (2011) for the spectral lines of interest were used as the a priori for the retrieved spectroscopic parameters. The line positions were left fixed to the values measured in Leshchishina et al. (2011), and all other O_2 spectral lines (intensity less 7.0×10^{-28} cm^{-1}/(molecule cm^{-2})) were calculated using a Voigt line shape with spectroscopic parameters from HITRAN 2012 (Rothman et al., 2013). Spectral fits were done using the lsqnonlin function in Matlab, with a user-defined Jacobian matrix. The Jacobian was constructed by taking the derivative of the absorption coefficients with respect to the parameters of interest. Using an analytical Jacobian instead of the finite difference method is both computationally faster and more accurate. The Voigt line shape was calculated using the Matlab code created by Abrarov and Quine (2011) to calculate the complex error function and its derivatives. To take collision-induced absorption (CIA) into account, a set of 50 Legendre polynomials were added together by retrieving the weighting coefficients needed to add the polynomials to fit the CIA for each spectrum. Figure 1b shows the residual (measured minus calculated absorption coefficients) when using a Voigt line shape with the retrieved spectroscopic parameters. The plot shows that residual structure still remains for all three spectra. The Root Mean Square (RMS) residual values for the spectra are given by the legend at the side of the plot.

Figure 2 is the same plot as Figure 1 but for the P(11)P(11), P(11)Q(10), P(9)P(9), and P(9)Q(8) spectral lines only. Figure 2b shows that for all four spectral lines there is a "W" shaped residual at the line center. The P(11)P(11) line

429 was also measured by Hartmann et al. (2013) at pressures ranging from 6.7 to 107 kPa. Figure 5 of Hartmann et al.

430 (2013) shows the P(11)P(11) line at a pressure of 66.7 kPa, which is approximately the pressure of the 66.9 kPa

431 spectrum (blue spectrum in Figure 1 and 2). When one compares the blue residual of the P(11)P(11) line in Figure

432 2b to that of the residual of the left panel of Figure 5 of Hartmann et al. (2013), one can see that the residuals are the

433 same. Figure 6 of Hartmann et al. (2013) show that the amplitude of the residual increases with decreasing pressure,

434 which is also seen in Figure 2b. Figure 3 of Lamouroux et al. (2014) shows the same "W" residual for the P(9)P(9)

435 lines and that the amplitude of the residual increases with decreasing pressure (although for lower pressures)

436 consistent with the results for the P(9)P(9) line in Figure 2b.

437 Figure 1c shows the residual when using the speed-dependent Voigt (Eq. 4) to fit each spectrum individually. To use

438 Eq. (4) requires integration over all possible speeds, which is not computationally practical, so we employ the

439 simple numerical integration scheme as was done by Wehr (2005). When fitting the spectra, parameters S_j, $\gamma_{L_j}^o$, δ_j^o,

440 $a_{\gamma_{L_i}}$ and a_{δ_j} were retrieved for lines of intensity greater than 7.0×10^{-28} cm^{-1}/(molecule cm^{-2}), while all other O_2 lines

441 were calculated using a Voigt line shape and spectroscopic parameters from HITRAN 2012 (Rothman et al., 2013b).

442 The Jacobian matrix was created by taking the derivative with respect to each parameter of interest, as was done

443 with the Voigt fits. By taking speed-dependent effects into account, the residuals were reduced to 25 times smaller

444 than those for the Voigt fit and the RMS residuals (given in the legend of Figure 1c) are 10 times smaller. However,

445 some residual structure still remains, which is more evident in the in the Q and R branches than the P branch. Figure

446 2c shows the four lines in the P branch, as discussed when analyzing the Voigt fits. A small residual "W" remains at

447 line center, as well as residuals from weak O_2 lines.

448 Figure 3 shows the averaged intensity, Lorentz width coefficient, pressure shift coefficient, and speed-dependent

449 shift coefficient of the 1.27 μm O_2 band, retrieved from the three spectra, plotted as a function of ~~J''.~~ quantum

450 number m which is m=-J (where J is the lower state rotational quantum number) for the P-branch lines, m=J for the

451 Q-branch lines, and m=J+1 for the R-branch lines. The intensity, Lorentz widths, and pressure shifts show a ~~J''~~ m

452 dependence for these parameters for the P and R sub-branches. The measured Lorentz widths and pressure shifts for

453 the Q sub-branches show a ~~J''~~ m dependence but are not as strong as the P and R sub-branches. This is because the

454 Q branch lines are broadened enough to blend with each other since they are spaced closer together than the P or R

455 branch lines. Figure 1c shows that some of the residual structure in the Q branch increases with pressure and is

456 partly due to the blending of these transitions as the pressure increases. The weak O_2 absorption lines also blend in

457 with the Q branch, contributing to the residual structure in Figure 1c. We tried retrieving the spectroscopic

458 parameters for the weak O_2 absorption lines, but since they were overlapping with the strong O_2 lines, it was not

459 possible. Figure 4a shows the retrieved speed-dependent width parameter averaged over the three spectra, plotted as

460 a function of ~~J''~~ m, showing that it increases with ~~J''~~ m. Error bars correspond to the 2σ standard deviation and are

461 large regardless of sub-branch. Figure 4b shows the retrieved speed-dependent width for the PQ sub-branch for the

462 different pressures. The speed-dependent width shows the same ~~J''~~ m dependence regardless of pressure, but also

463 increases with decreasing pressure as is the case for sub-branches. It should be noted that the speed-dependent width

464 parameter should be independent of pressure.

4. Fitting Solar Spectra

465

466 High-resolution solar absorption spectra were measured at four TCCON sites using a Bruker IFS 125HR FTIR

467 spectrometer with a room temperature InGaAs detector at a spectral resolution of 0.02 cm^{-1} (45 cm maximum

468 optical path difference). The raw interferograms recorded by the instrument were processed into spectra using the

469 I2S software package (Wunch, D. et al., 2015) that corrects them for solar intensity variations (Keppel-Aleks et al.,

470 2007), phase errors (Mertz, 1967), and laser sampling errors (Wunch, D. et al., 2015), and then preforms a fast

471 Fourier transforms to convert the interferograms into spectra (Bergland, 1969). The GGG software package (Wunch,

472 D. et al., 2015) is used to retrieve total columns of atmospheric trace gases. GFIT is the main code that contains the

473 forward model, which calculates a solar absorption spectrum using a line-by-line radiative transfer model and an

474 iterative non-linear least square fitting algorithm that scales an a priori gas profile to obtain the best fit to the

475 measured spectrum. A priori profiles for GHGs are created by an empirical model in GGG that is based on

476 measurements from the balloon-borne JPL MkIV Fourier Transform Spectrometer (FTS) (Toon, 1991), the

477 Atmospheric Chemistry Experiment (ACE) FTS instrument aboard SCISAT (Bernath et al., 2005), and in situ

478 GLOBALVIEW data (Wunch et al., 2011). Temperature and pressure profiles, as well as H_2O a priori profiles are

479 generated from the National Centers for Environmental Prediction (NCEP) data. The calculations are performed for

480 71 atmospheric layers (0 km to 70 km), so all a priori profiles are generated on a vertical grid of 1 km.

481 In the current GGG software package (Wunch, D. et al., 2015), the forward model of GFIT calculates absorption

482 coefficients for the discrete lines of the O_2 1.27 µm band using a Voigt line shape and spectroscopic parameters

483 from Washenfelder et al. (2006a) and Gordon et al. (2010). To take CIA into account, absorption coefficients are

484 calculated using a Voigt line shape and spectroscopic parameters from the foreign-collision-induced absorption

485 (FCIA) and self-collision-induced absorption (SCIA) spectral line lists provided with the GGG software package

486 (Wunch, D. et al., 2015). Spectroscopic parameters in the FCIA and SCIA line lists were retrieved by Geoff Toon by

487 fitting the laboratory spectra of Smith and Newnham (2000). This was done by retrieving the integrated absorption

488 at every 1 cm^{-1} of the spectrum and using a Voigt line shape, with fixed Lorentz width and no pressure shift. In

489 GFIT, a volume scale factor is retrieved for the CIA and discrete lines separately so that the O_2 column is derived

490 from the discrete lines of the 1.27 µm band only. Airglow is not considered when fitting the 1.27 µm band since the

491 spectrometer views the sun directly, and airglow is overwhelmed by such a bright source. The continuum level and

492 tilt of the 100% transmission level is fitted using a weighted combination of the first two Legendre polynomials.

493 Absorption coefficient for all other trace gases are calculated using a Voigt line shape and spectroscopic parameters

494 from the atm.101 line list (Toon, G. C., 2014a)(Wunch, D. et al., 2015) and solar lines are fitted using the solar line

495 list (Toon, G. C., 2014b)(Wunch, D. et al., 2015).

496 Figure 5 shows the spectral fit to a solar absorption spectrum recorded at Eureka on March 27, 2015, at a solar

497 zenith angle (SZA) of 81.32° (airmass of 6.3). This spectrum is an average of 5 Eureka scans. The TCCON standard

498 is single scan but 5 scans were averaged to decrease the noise. The measured spectrum (red circles), calculated

499 spectrum (black circles) and transitions from all gases in the window (colored lines, refer to the legend for different

500 gases) are shown in Figure 5b. The residual obtained using a Voigt line shape to calculate the discrete lines of the O_2

501   1.27 µm band is shown in red in Figure 5a. The blue residual is the result of using a speed-dependent Voigt line

502   shape with the spectroscopic parameters retrieved from fitting the absorption coefficients in Section 3. To decrease

503   the amount of time it takes to calculate the absorption coefficients, the quadratic-Speed Dependent Voigt (qSDV)

504   computational approach of Ngo et al. (2013) and Tran et al. (2013)was used instead of Eq. (4) since it requires the

505   Voigt calculation only twice, while Eq. (4) requires numerical integration scheme with 33 iterations. The

506   temperature-dependent parameter of the Lorentz width of the discrete lines of the O_2 1.27 µm band reported in

507   HITRAN 2012 was used to take temperature dependence into account for $\gamma_{L_j}(T)$. There was only a slight

508   improvement in the fit residuals with the new absorption coefficients (using the qSDV), as seen in Figure 5a.

509   Absorption coefficients calculated with the qSDV were used to retrieve total columns of O_2 from solar spectra

510   recorded over a one year period at TCCON sites in Eureka (eu) (Nunavut, Canada) (Batchelor et al., 2009; Strong et

511   al., 2017)(Batchelor et al., 2009), Park Falls (pa) (Wisconsin, U.S.A) (Washenfelder et al., 2006; Wennberg et al.,

512   2017)(Washenfelder et al., 2006b), Lamont (oc) (Oklahoma, U.S.A) (Wennberg et al., 2017b), and Darwin (db)

513   (Australia) (Deutscher et al., 2010; Griffith et al., 2017)(Deutscher et al., 2010). In total 131 124 spectra were fitted

514   using the qSDV and the average root mean square (RMS) residual of the fit only decreased by 0.5 %.

515   **5. Impact of O_2 Columns on XCO$_2$ Measurements**

516   The O_2 column retrieved from the 1.27 µm band with a Voigt line shape and spectroscopic parameters from the

517   atm.101 line list (Toon, G. C., 2014a) (Wunch, D. et al., 2015) has an airmass dependence such that the O_2 column

518   retrieved increases as a function of solar zenith angle (or airmass). Using spectra recorded from Eureka, Park Falls,

519   Lamont, and Darwin over one-year periods, total columns of O_2 were retrieved using (1) a Voigt spectral line shape

520   with spectroscopic parameters from the atm.101 line list and (2) the qSDV with the spectroscopic parameters

521   determined in Section 3. Figure 6 shows the percent difference calculated as the column from the qSDV retrieval

522   minus the column from the Voigt retrieval, which was then divided by the latter and multiplied by 100, plotted as a

523   function of solar zenith angle (SZA). At the smallest SZA, the qSDV retrieves 0.75% less O_2 than the Voigt, with

524   the difference increasing to approximately 1.8% as the SZA approaches 90º. Figure 7 shows XAIR from Park Falls

525   on June 18, 2013. XAIR is the column of air (determined using surface pressure recorded at the site) divided by the

526   column of O_2 retrieved from the spectra and multiplied by 0.2095, which is the dry air mole fraction of O_2 in Earth's

527   atmosphere. Ideally XAIR should be 1 but when using O_2 retrieved with a Voigt line shape (red points) it is closer to

528   0.98 near noon (small SZA) and lower near the start and end of the day (large SZA). When using O_2 retrieved with

529   the qSDV, XAIR is closer to 0.988 near noon and a bit higher near the start and end of the day. This means the O_2

530   column, retrieved with the qSDV, decreases as a function of SZA, while previously the column increased as a

531   function of SZA when the Voigt line shape is used.

532   **5.1 Airmass Dependence of XCO$_2$**

533   Since the standard TCCON XCO$_2$ (and all other XGas) is calculated using the column of O_2 instead of the surface

534   pressure, errors associated with the retrieval of O_2, such as the airmass dependence of the O_2 column, will affect

535   XCO$_2$. Figure 8 is XCO$_2$ calculated for four different combinations pertaining to the two CO$_2$ column retrievals and

the O_2 column retrievals. The CO_2 columns were retrieved with either a Voigt line shape (the standard GGG2014 approach) or the qSDV with line mixing as done in Mendonca et al. (2016) while the O_2 columns were retrieved with either a Voigt (the standard GGG2014 approach) or the new qSDV approach developed here. Figure 8 shows a spurious symmetric component to XCO_2 when the total column of O_2 is retrieved with the Voigt line shape, regardless of line shape used to retrieve CO_2. When the qSDV is used to retrieve total columns of O_2, the symmetric component of XCO_2 is dismissed regardless of line shape used to retrieve CO_2. This is because the airmass dependence of the column of O_2 retrieved using the qSDV is more consistent with the airmass dependence of the column of CO_2 (for both line shapes used to retrieve CO_2). Mendonca et al. (2016) showed that using the qSDV with line mixing results in better fits to the CO_2 windows and impacts the airmass dependence of the retrieved column of CO_2. When using a Voigt line shape the retrieved column amount of CO_2 decreases as airmass increases until the airmass is large (SZA of about 82°) at which point the retrieved column of CO_2 increases as the airmass increases, changing the shape of the airmass dependence of the CO_2 column. When the qSDV with line mixing is used, the retrieved column of CO_2 decreases as a function of airmass (up until the sun is above the horizon).

~~In order to~~ To correct for this, an empirical correction is applied to all TCCON XCO_2 (and XGas). The empirical correction determines the antisymmetrical component of the day's XCO_2, which is assumed to be the true variation of XCO_2 throughout the day, as well as the symmetrical component, which is caused by the airmass dependence of the retrieved column of the gas of interest and O_2. We can, therefore, represent a measurement as (Wunch et al., 2011):

$$y_i = \hat{y}[1 + \alpha S(\theta_i) + \beta A(t_i)] \tag{5}$$

where $\hat{y}$ is the mean value of XCO_2 measured that day, β is the fitted coefficient of the antisymmetric function $A(t_i)$ and α is the fitted coefficient of the symmetric function $S(\theta_i)$. The antisymmetric function is calculated by (Wunch et al., 2011):

$$A(t_i) = \sin(2\pi(t_i - t_{noon})) \tag{6}$$

where t_i is the time of the measurement and t_{noon} is the time at solar noon, both in units of days. The symmetric function is calculated by (Wunch et al., 2011):

$$S(\theta_i) = \left(\frac{\theta_i + 13^o}{90^o + 13^o}\right)^3 - \left(\frac{\theta_t 45^o + 13^o}{90^o + 13^o}\right)^3 \tag{7}$$

where θ_i is the SZA in degrees. To determine α for the different line shapes, total columns of CO_2 were retrieved using the Voigt line shape (Wunch, D. et al., 2015) and the qSDV with line mixing (Mendonca et al., 2016). Henceforth, we will refer to XCO_2 calculated from O_2 and CO_2 using the Voigt line shape as XCO_2 Voigt and the qSDV line shape as XCO_2 qSDV.

Figure 97 shows the average α calculated for each season at Darwin, Lamont, and Park Falls. Eureka XCO_2 cannot be used to determine α because Eureka measurements do not go through the same range of SZAs as the other three

565   sites due to its geolocation. The average α values derived from XCO_2 Voigt are represented by stars in Figure 9~~7~~,

566   while the squares indicate XCO_2 qSDV. At all three sites, α is closer to 0 when the qSDV line shape is used in the

567   retrieval compared to the Voigt retrieval, regardless of the season. The average α for XCO_2 Voigt calculated from a

568   year of measurements from Darwin, Park Falls, and Lamont is -0.0071±0.0057 and that for XCO_2 qSDV is -

569   0.0012±0.0054.

570   For all four sites, α = -0.0071 is used to correct XCO_2 Voigt measurements. Figure 10~~8~~a shows the XCO_2 Voigt

571   anomalies plotted as a function of SZA. The data is expressed as the daily XCO_2 anomaly, which is the difference

572   between the XCO_2 value and the daily median value, in order to remove the seasonal cycle. When XCO_2 is left

573   uncorrected for airmass dependencies, ~~there is a clear airmass dependence where the amount of~~ XCO_2 decreases as a

574   function of SZA up to ~~a SZA of~~ approximately 82°, ~~at which point XCO₂~~ and increases as a function of SZA at

575   andgles greater than 82°. Figure 10~~8~~b shows XCO_2 Voigt corrected for the airmass dependence. This airmass

576   correction works well only up to a SZA of approximately 82°, ~~after which the correction only serves to increase the~~

577   ~~airmass dependence~~. Figure 10~~8~~c is the same as 10~~8~~a but for the uncorrected XCO_2 qSDV measurements, while

578   Figure 10~~8~~d is the same as 10~~8~~b but for the corrected XCO_2 qSDV measurements. When the airmass correction is

579   applied to XCO_2 qSDV there is a small difference between the corrected and uncorrected XCO_2 qSDV

580   measurements, with the difference only noticeable for the Darwin measurements recorded at SZA > 60°. For XCO_2

581   qSDV measurements made at SZA > 82° XCO_2 does not increase with SZA as it does with the Voigt.

5.2 Accuracy of XCO_2

583   To assess the accuracy of TCCON XCO_2 measurements, they are compared to aircraft XCO_2 profile measurements

584   using the method described in Wunch et al. (2010). Figure 11~~9~~a shows the comparison between the aircraft XCO_2

585   measurements (legend ~~on~~ at the top details the different aircraft) and TCCON XCO_2 Voigt measurements for 13

586   TCCON sites (given by the color-coded legend ~~on~~ at the bottom right). The gray line indicates the one-to-one line

587   and the dashed line is the line of best fit. There is a bias of 0.9897±0.0005, as given by the slope of the line of best

588   fit in Figure 11~~9~~a, for the XCO_2 Voigt measurements. Figure 11~~9~~b is the same as 11~~9~~a but for the XCO_2 qSDV

589   measurements. The bias between the aircraft XCO_2 measurements and the XCO_2 qSDV measurements is

590   1.0041±0.0005 as given by the slope of the line of best fit in Figure 11~~9~~b. This increase in the slope can be

591   explained by an increase in the retrieved column of CO_2 when using the qSDV with line mixing as shown in

592   Mendonca et al. (2016) as well as combined with a decrease in the retrieved O_2 column due to using the qSDV. As

593   discussed previously (section 5) the decrease in the retrieved O_2 column is an improvement but the expected column

594   of O_2 is still approximately 1.2% higher (at the smallest SZA) than it should be. Therefore, the retrieved column of

595   CO_2 is higher than it should be, and the slope would be greater if the retrieved column of O_2 was 1.2% lower. Never

596   the less ~~Using~~ using the qSDV to retrieve total columns of CO_2 and O_2 ~~thus~~ reduces the difference between TCCON

597   XCO_2 and aircraft XCO_2 measurements by 0.62 %.

598   TCCON XCO_2 measurements are divided by the scale factors (or bias determined in Figure 11~~9~~) to calibrate to the

599   WMO scale. For all TCCON XCO_2 measurements retrieved with a Voigt line shape, the airmass correction is first

600 applied to the data and the result is divided by the determined bias factor, 0.9897. Figure 12~~10~~a to 12~~10~~d shows

601 XCO_2 Voigt (for Eureka, Park Falls, Lamont, and Darwin respectively) indicated by red square boxes in the plots.

602 XCO_2 Voigt measurements made at SZA > 82º have been filtered out because they cannot be corrected for the

603 airmass dependence. The blue boxes are XCO_2 qSDV corrected for airmass dependence and scaled by 1.0041. No

604 filter was applied to the XCO_2 qSDV measurements for SZA since the airmass dependence correction works at all

605 SZA. Figure 12~~10~~e to 12~~10~~h shows the difference between XCO_2 Voigt and XCO_2 qSDV for Eureka, Park Falls,

606 Lamont, and Darwin respectively. The mean differences for the data shown in Figures 12~~10~~e to 12~~10~~h are

607 0.113±0.082, -0.102±0.223, -0.132±0.241, and -0.059±0.231 µmol/mol (ppm) for Eureka, Park Falls, Lamont, and

608 Darwin respectively. The difference throughout the day at Park Falls, Lamont, and Darwin varies between -0.6 to

609 0.2 µmol/mol and is SZA dependent.

610 Figure 13~~11~~a shows XCO_2 Voigt corrected for the airmass dependence, as well as XCO_2 qSDV, uncorrected and

611 corrected for the airmass dependence. These XCO_2 measurements were retrieved from Park Falls spectra recorded

612 on June 18, 2013. For all three XCO_2 measurements, the amount of XCO_2 decreases throughout the day. Figure

613 13~~11~~b shows the difference between the corrected Voigt XCO_2 and the uncorrected qSDV XCO_2, as well as the

614 difference between the corrected Voigt XCO_2 and the corrected qSDV XCO_2. The difference between the Voigt and

615 the qSDV (corrected and uncorrected) shows that at the start and end of the day, more XCO_2 is retrieved with the

616 qSDV, while at midday less is retrieved with the qSDV. The range in the differences seen in Figure 12~~10~~e to 12~~10~~h

617 varies with SZA throughout the day as shown in Figure 13~~11~~b.

618 **6. Discussion and Conclusions**

619 Using cavity ring-down spectra measured in the lab, we have shown that the Voigt line shape is insufficient to

620 model the line shape of O_2 for the 1.27 µm band, consistent with the results of(Hartmann et al. (2013) and

621 Lamouroux et al. (2014). By using the speed-dependent Voigt line shape when calculating the absorption

622 coefficients, we were better able to reproduce the measured absorption coefficients than using the Voigt line shape.

623 However, some residual structure ~~still~~ remains as seen Figures 1 and 2. This is partly due to the blending of spectral

624 lines (i.e., line mixing) and the inability to retrieve the spectroscopic parameters for weak O_2 transitions. Fitting low-

625 pressure spectra would help with isolating spectral lines and decreasing the uncertainty on the retrieved

626 spectroscopic parameters for the Q branch lines.

627 Accurate measurements of the pressure shifts in the 1.27 µm band have been hard to obtain as shown in Newman et

628 al. (1999) and Hill et al., (2003). While the retrieved pressure shifts show a dependence on quantum number m

629 (Figure 3c) as one would expect, this dependence is not as strong as the m dependence of the Lorentz widths (Figure

630 3b). This can be explained by the fact that line mixing, which is shown to be important for the O_2 A-band, was not

631 considered when fitting the cavity-ringdown spectra. Neglecting line mixing usually produces an asymmetric

632 residual in the discrete lines as well as a broad residual feature associated with the fact that collisions are transferring

633 intensity from one part of the spectrum to another. By fitting a set of Legendre polynomials for CIA we could be

634 simultaneously fitting the broader band feature associated with line mixing while the retrieved pressure shifts, and

635 speed-dependent pressure shifts could be compensating for the asymmetric structure one would see in the discrete
636 lines when neglecting line mixing. The remaining structure, as seen in Figure 1c, could be due to neglecting line
637 mixing especially in the Q-branch where the spacing between spectral lines is small (in comparison to the P and R
638 branches) and line mixing is most likely prevalent.

639 The pressure dependence of the retrieved speed-dependent width parameter is an indication that Dicke narrowing
640 needs to be taken into account, as shown by Bui et al. (2014) for CO_2. However, when When dealing with both
641 speed dependence and Dicke narrowing are present, a multi-spectrum fit needs to be used due to the correlation
642 between the parameters (Bui et al., 2014). Domysławska et al. (2016) recommend using the qSDV to model the line
643 shape of O_2 based on multiple line shape studies of the O_2 B-band. In these studies, a multi-spectrum fit to low
644 pressure (0.27-5.87 kPa) cavity-ring down spectra was preformed testing multiple line shapes that took speed-
645 dependence and Dicke narrowing into account both separately and simultaneously. They found that the line shapes
646 that only used Dicke narrowing were not good enough to model the line shape of the O_2 B-band lines, but a line
647 shape that included either speed-dependence or both speed-dependence and Dicke narrowing produced similar
648 quality fits, ultimately concluding that speed-dependence has a larger effect than Dicke narrowing. It was noted in
649 the study by Wójtewicz et al., (2014) that both Dicke narrowing and speed-dependent effects might simultaneously
650 play an important role in modeling the line shape of the O_2 B-band lines. However, the speed-dependent and Dicke
651 narrowing parameters are highly correlated at low pressures. To reduce the correlation requires either a multi-
652 spectrum fit of spectra at low pressures with high enough signal to nosie ratio or spectra that cover a wide range of
653 pressure (Wójtewicz et al., 2014). So, by combining the high-pressure spectra used in this study with low pressure
654 spectra in a multipspectrum fit both the speed-dependence and Dicke narrowing parameters could be retrieved. The
655 temperature dependence of the Lorentz width coefficients of this band has never been measured before, which could
656 have an impact on the airmass dependence of O_2. Combining high-pressure cavity-ring-down absorption coefficient
657 measurements with those for low pressures and different temperatures as done in Devi et al. (2015 and 2016) for
658 CH_4 in would lead to more accurate line shape parameters for O_2.

659 By taking speed dependence into account for both CO_2 (in the work of Mendonca et al., 2016) and O_2 (the work
660 presented here), we were able to significantly decrease the airmass dependence of TCCON XCO_2 and the bias
661 between TCCON and aircraft XCO_2. With the qSDV line shape, XCO_2 measurements made at SZA > 82º no longer
662 have to be discarded, resulting in more XCO_2 measurement available from all TCCON sites. This is particularly
663 important for high-latitude TCCON sites, such as Eureka, because measurements made from late February to late
664 March and from late September until mid-October are made at SZA > 82º. Filtering out these large SZA
665 measurements thus limits the knowledge of the seasonal cycle of XCO_2 at high latitudes. The airmass dependence of
666 the O_2 column not only effects XCO_2 but all trace gases measured by TCCON and in the future the airmass
667 dependence of all XGas will be determined with these new O_2 columns.

668 **Acknowledgements**

688

689

690

691

692

693

694

695

696

697

698

699

700

References

Abrarov, S.M., Quine, B.M., 2011. Efficient algorithmic implementation of the Voigt/complex error function based on exponential series approximation. Appl. Math. Comput. 218, 1894–1902. https://doi.org/10.1016/j.amc.2011.06.072

Batchelor, R.L., Strong, K., Lindenmaier, R., Mittermeier, R.L., Fast, H., Drummond, J.R., Fogal, P.F., 2009. A New Bruker IFS 125HR FTIR Spectrometer for the Polar Environment Atmospheric Research Laboratory at Eureka, Nunavut, Canada: Measurements and Comparison with the Existing Bomem DA8 Spectrometer. J. Atmospheric Ocean. Technol. 26, 1328–1340. https://doi.org/10.1175/2009JTECHA1215.1

Bergland, G., 1969. A radix-eight fast Fourier transform subroutine for real-valued series. IEEE Trans. Audio Electroacoustics 17, 138–144. https://doi.org/10.1109/TAU.1969.1162043

Bernath, P.F., McElroy, C.T., Abrams, M.C., Boone, C.D., Butler, M., Camy-Peyret, C., Carleer, M., Clerbaux, C., Coheur, P.-F., Colin, R., DeCola, P., DeMazière, M., Drummond, J.R., Dufour, D., Evans, W.F.J., Fast, H., Fussen, D., Gilbert, K., Jennings, D.E., Llewellyn, E.J., Lowe, R.P., Mahieu, E., McConnell, J.C., McHugh, M., McLeod, S.D., Michaud, R., Midwinter, C., Nassar, R., Nichitiu, F., Nowlan, C., Rinsland, C.P., Rochon, Y.J., Rowlands, N., Semeniuk, K., Simon, P., Skelton, R., Sloan, J.J., Soucy, M.-A., Strong, K., Tremblay, P., Turnbull, D., Walker, K.A., Walkty, I., Wardle, D.A., Wehrle, V., Zander, R., Zou, J., 2005. Atmospheric Chemistry Experiment (ACE): Mission overview. Geophys. Res. Lett. 32, L15S01. https://doi.org/10.1029/2005GL022386

Bui, T.Q., Long, D.A., Cygan, A., Sironneau, V.T., Hogan, D.W., Rupasinghe, P.M., Ciuryło, R., Lisak, D., Okumura, M., 2014. Observations of Dicke narrowing and speed dependence in air-broadened CO_2 lineshapes near 2.06 μm. J. Chem. Phys. 141, 174301. https://doi.org/10.1063/1.4900502

Cheah, S.-L., Lee, Y.-P., Ogilvie, J.F., 2000. Wavenumbers, strengths, widths and shifts with pressure of lines in four bands of gaseous $^{16}O_2$ in the systems $a^1\Delta_g-X^3\Sigma_g^-$ and $b^1\Sigma_g^+-X^3\Sigma_g^-$. J. Quant. Spectrosc. Radiat. Transf. 64, 467–482. https://doi.org/10.1016/S0022-4073(99)00126-0

Ciuryło, R., 1998. Shapes of pressure- and Doppler-broadened spectral lines in the core and near wings. Phys. Rev. A 58, 1029–1039. https://doi.org/10.1103/PhysRevA.58.1029

Crisp, D., Atlas, R.M., Breon, F.-M., Brown, L.R., Burrows, J.P., Ciais, P., Connor, B.J., Doney, S.C., Fung, I.Y., Jacob, D.J., Miller, C.E., O'Brien, D., Pawson, S., Randerson, J.T., Rayner, P., Salawitch, R.J., Sander, S.P., Sen, B., Stephens, G.L., Tans, P.P., Toon, G.C., Wennberg, P.O., Wofsy, S.C., Yung, Y.L., Kuang, Z., Chudasama, B., Sprague, G., Weiss, B., Pollock, R., Kenyon, D., Schroll, S., 2004. The Orbiting Carbon Observatory (OCO) mission. Adv. Space Res., Trace Constituents in the Troposphere and Lower Stratosphere 34, 700–709. https://doi.org/10.1016/j.asr.2003.08.062

Deutscher, N.M., Griffith, D.W.T., Bryant, G.W., Wennberg, P.O., Toon, G.C., Washenfelder, R.A., Keppel-Aleks, G., Wunch, D., Yavin, Y., Allen, N.T., Blavier, J.-F., Jiménez, R., Daube, B.C., Bright, A.V., Matross, D.M., Wofsy, S.C., Park, S., 2010. Total column CO_2 measurements at Darwin, Australia – site description and calibration against in situ aircraft profiles. Atmos Meas Tech 3, 947–958. https://doi.org/10.5194/amt-3-947-2010

Devi, V.M., Benner, D.C., Sung, K., Brown, L.R., Crawford, T.J., Yu, S., Smith, M.A.H., Mantz, A.W., Boudon, V., Ismail, S., 2016. Spectral line parameters including line shapes in the $2\nu_3$ Q branch of $^{12}CH_4$. J. Quant. Spectrosc. Radiat. Transf., XVIIIth Symposium on High Resolution Molecular Spectroscopy (HighRus-2015), Tomsk, Russia 177, 152–169. https://doi.org/10.1016/j.jqsrt.2015.12.009

Devi, V.M., Benner, D.C., Sung, K., Crawford, T.J., Yu, S., Brown, L.R., Smith, M.A.H., Mantz, A.W., Boudon, V., Ismail, S., 2015. Self- and air-broadened line shapes in the $2\nu_3$ P and R branches of 12CH4. J. Mol. Spectrosc., Spectroscopy with Synchrotron Radiation 315, 114–136. https://doi.org/10.1016/j.jms.2015.05.003

Dicke, R.H., 1953. The Effect of Collisions upon the Doppler Width of Spectral Lines. Phys. Rev. 89, 472–473. https://doi.org/10.1103/PhysRev.89.472

Domysławska, J., Wójtewicz, S., Masłowski, P., Cygan, A., Bielska, K., Trawiński, R.S., Ciuryło, R., Lisak, D., 2016. A new approach to spectral line shapes of the weak oxygen transitions for atmospheric applications. J. Quant. Spectrosc. Radiat. Transf. 169, 111–121. https://doi.org/10.1016/j.jqsrt.2015.10.019

Drouin, B.J., Benner, D.C., Brown, L.R., Cich, M.J., Crawford, T.J., Devi, V.M., Guillaume, A., Hodges, J.T., Mlawer, E.J., Robichaud, D.J., Oyafuso, F., Payne, V.H., Sung, K., Wishnow, E.H., Yu, S., 2017.

Multispectrum analysis of the oxygen A-band. J. Quant. Spectrosc. Radiat. Transf., Satellite Remote Sensing and Spectroscopy: Joint ACE-Odin Meeting, October 2015 186, 118–138. https://doi.org/10.1016/j.jqsrt.2016.03.037

Gordon, I.E., Kassi, S., Campargue, A., Toon, G.C., 2010. First identification of the electric quadrupole transitions of oxygen in solar and laboratory spectra. J. Quant. Spectrosc. Radiat. Transf., Special Issue Dedicated to Laurence S. Rothman on the Occasion of his 70th Birthday. 111, 1174–1183. https://doi.org/10.1016/j.jqsrt.2010.01.008

Gordon, I.E., Rothman, L.S., Hill, C., Kochanov, R.V., Tan, Y., Bernath, P.F., Birk, M., Boudon, V., Campargue, A., Chance, K.V., Drouin, B.J., Flaud, J.-M., Gamache, R.R., Hodges, J.T., Jacquemart, D., Perevalov, V.I., Perrin, A., Shine, K.P., Smith, M.-A.H., Tennyson, J., Toon, G.C., Tran, H., Tyuterev, V.G., Barbe, A., Császár, A.G., Devi, V.M., Furtenbacher, T., Harrison, J.J., Hartmann, J.-M., Jolly, A., Johnson, T.J., Karman, T., Kleiner, I., Kyuberis, A.A., Loos, J., Lyulin, O.M., Massie, S.T., Mikhailenko, S.N., Moazzen-Ahmadi, N., Müller, H.S.P., Naumenko, O.V., Nikitin, A.V., Polyansky, O.L., Rey, M., Rotger, M., Sharpe, S.W., Sung, K., Starikova, E., Tashkun, S.A., Auwera, J.V., Wagner, G., Wilzewski, J., Wcisło, P., Yu, S., Zak, E.J., 2017. The HITRAN2016 molecular spectroscopic database. J. Quant. Spectrosc. Radiat. Transf., HITRAN2016 Special Issue 203, 3–69. https://doi.org/10.1016/j.jqsrt.2017.06.038

Griffith, D.W.T., Deutscher, N.M., Velazco, V.A., Wennberg, P.O., Yavin, Y., Keppel-Aleks, G., Washenfelder, R.A., Toon, G.C., Blavier, J.-F., Paton-Walsh, C., Jones, N.B., Kettlewell, G.C., Connor, B.J., Macatangay, R.C., Roehl, C., Ryczek, M., Glowacki, J., Culgan, T., Bryant, G.W., 2017. TCCON data from Darwin (AU), Release GGG2014.R0. https://doi.org/10.14291/tccon.ggg2014.darwin01.R0/1149290

Hartmann, J.-M., Sironneau, V., Boulet, C., Svensson, T., Hodges, J.T., Xu, C.T., 2013. Collisional broadening and spectral shapes of absorption lines of free and nanopore-confined O_2 gas. Phys. Rev. A 87, 032510. https://doi.org/10.1103/PhysRevA.87.032510

Hill, C., Brown, J.M., Newnham, D.A., 2003. An upper limit for the magnitude of pressure shifts in the O_2 $a^1\Delta_g \leftarrow X^3\Sigma_g^-(0–0)$ band. J. Mol. Spectrosc. 221, 286–287. https://doi.org/10.1016/S0022-2852(03)00227-3

Hodges, J.T., 2005. Automated high-resolution frequency-stabilized cavity ring-down absorption spectrometer. Rev. Sci. Instrum. 76, 023112. https://doi.org/10.1063/1.1850633

Hodges, J.T., Layer, H.P., Miller, W.., Scace, G.E., 2004. Frequency-stabilized single-mode cavity ring-down apparatus for high-resolution absorption spectroscopy. Rev. Sci. Instrum. 75, 849–863. https://doi.org/10.1063/1.1666984

Keppel-Aleks, G., Toon, G.C., Wennberg, P.O., Deutscher, N.M., 2007. Reducing the impact of source brightness fluctuations on spectra obtained by Fourier-transform spectrometry. Appl. Opt. 46, 4774. https://doi.org/10.1364/AO.46.004774

Lamouroux, J., Sironneau, V., Hodges, J.T., Hartmann, J.-M., 2014. Isolated line shapes of molecular oxygen: Requantized classical molecular dynamics calculations versus measurements. Phys. Rev. A 89, 042504. https://doi.org/10.1103/PhysRevA.89.042504

Leshchishina, O., Kassi, S., Gordon, I.E., Rothman, L.S., Wang, L., Campargue, A., 2010. High sensitivity CRDS of the $a^1\Delta_g - X^3\Sigma_g^-$ band of oxygen near 1.27 µm: Extended observations, quadrupole transitions, hot bands and minor isotopologues. J. Quant. Spectrosc. Radiat. Transf., XVIth Symposium on High Resolution Molecular Spectroscopy (HighRus-2009) XVIth Symposium on High Resolution Molecular Spectroscopy 111, 2236–2245. https://doi.org/10.1016/j.jqsrt.2010.05.014

Leshchishina, O., Kassi, S., Gordon, I.E., Yu, S., Campargue, A., 2011. The band of $^{16}O^{17}O$, $^{17}O^{18}O$ and $^{17}O_2$ by high sensitivity CRDS near 1.27 µm. J. Quant. Spectrosc. Radiat. Transf. 112, 1257–1265. https://doi.org/10.1016/j.jqsrt.2011.01.014

Lévy, A., Lacome, N., Chackerian Jr., C., 1992. Collisional Line Mixing A2 - Weber, K. Narahari RaoAlfons, in: Spectroscopy of the Earth's Atmosphere and Interstellar Medium. Academic Press, pp. 261–337.

Lin, H., Reed, Z.D., Sironneau, V.T., Hodges, J.T., 2015. Cavity ring-down spectrometer for high-fidelity molecular absorption measurements. J. Quant. Spectrosc. Radiat. Transf. 161, 11–20. https://doi.org/10.1016/j.jqsrt.2015.03.026

Long, D.A., Havey, D.K., Okumura, M., Miller, C.E., Hodges, J.T., 2010. O_2 A-band line parameters to support atmospheric remote sensing. J. Quant. Spectrosc. Radiat. Transf. 111, 2021–2036. https://doi.org/10.1016/j.jqsrt.2010.05.011

Maté, B., Lugez, C., Fraser, G.T., Lafferty, W.J., 1999. Absolute intensities for the O_2 1.27 µm continuum absorption. J. Geophys. Res. Atmospheres 104, 30585–30590. https://doi.org/10.1029/1999JD900824

Mendonca, J., Strong, K., Toon, G.C., Wunch, D., Sung, K., Deutscher, N.M., Griffith, D.W.T., Franklin, J.E., 2016. Improving atmospheric CO_2 retrievals using line mixing and speed-dependence when fitting high-

resolution ground-based solar spectra. J. Mol. Spectrosc., Atmospheric Spectroscopy 323, 15–27. https://doi.org/10.1016/j.jms.2016.01.007

Mertz, L., 1967. Auxiliary computation for Fourier spectrometry. Infrared Phys. 7, 17–23. https://doi.org/10.1016/0020-0891(67)90026-7

Mlawer, E.J., Clough, S.A., Brown, P.D., Stephen, T.M., Landry, J.C., Goldman, A., Murcray, F.J., 1998. Observed atmospheric collision-induced absorption in near-infrared oxygen bands. J. Geophys. Res. Atmospheres 103, 3859–3863. https://doi.org/10.1029/97JD03141

Newman, S.M., Lane, I.C., Orr-Ewing, A.J., Newnham, D.A., Ballard, J., 1999. Integrated absorption intensity and Einstein coefficients for the O_2 $a^1\Delta_g$–$X^3\Sigma_g^-$ (0,0) transition: A comparison of cavity ringdown and high resolution Fourier transform spectroscopy with a long-path absorption cell. J. Chem. Phys. 110, 10749–10757. https://doi.org/10.1063/1.479018

Newman, S.M., Orr-Ewing, A.J., Newnham, D.A., Ballard, J., 2000. Temperature and pressure dependence of line widths and integrated absorption intensities for the O_2 $a^1\Delta_g$ - $X^3\Sigma_g^-$ (0,0) transition. J. Phys. Chem. A 104, 9467–9480.

Ngo, N.H., Lisak, D., Tran, H., Hartmann, J.-M., 2013. An isolated line-shape model to go beyond the Voigt profile in spectroscopic databases and radiative transfer codes. J. Quant. Spectrosc. Radiat. Transf. 129, 89–100. https://doi.org/10.1016/j.jqsrt.2013.05.034

Predoi-Cross, A., Hambrook, K., Keller, R., Povey, C., Schofield, I., Hurtmans, D., Over, H., Mellau, G.C., 2008. Spectroscopic lineshape study of the self-perturbed oxygen A-band. J. Mol. Spectrosc. 248, 85–110. https://doi.org/10.1016/j.jms.2007.11.007

Rohart, F., Mäder, H., Nicolaisen, H.-W., 1994. Speed dependence of rotational relaxation induced by foreign gas collisions: Studies on CH_3F by millimeter wave coherent transients. J. Chem. Phys. 101, 6475–6486. https://doi.org/10.1063/1.468342

Rothman, L.S., Gordon, I.E., Babikov, Y., Barbe, A., Chris Benner, D., Bernath, P.F., Birk, M., Bizzocchi, L., Boudon, V., Brown, L.R., Campargue, A., Chance, K., Cohen, E.A., Coudert, L.H., Devi, V.M., Drouin, B.J., Fayt, A., Flaud, J.-M., Gamache, R.R., Harrison, J.J., Hartmann, J.-M., Hill, C., Hodges, J.T., Jacquemart, D., Jolly, A., Lamouroux, J., Le Roy, R.J., Li, G., Long, D.A., Lyulin, O.M., Mackie, C.J., Massie, S.T., Mikhailenko, S., Müller, H.S.P., Naumenko, O.V., Nikitin, A.V., Orphal, J., Perevalov, V., Perrin, A., Polovtseva, E.R., Richard, C., Smith, M.A.H., Starikova, E., Sung, K., Tashkun, S., Tennyson, J., Toon, G.C., Tyuterev, V.G., Wagner, G., 2013b. The HITRAN2012 molecular spectroscopic database. J. Quant. Spectrosc. Radiat. Transf., HITRAN2012 special issue 130, 4–50. https://doi.org/10.1016/j.jqsrt.2013.07.002

Rothman, L.S., Gordon, I.E., Barbe, A., Benner, D.C., Bernath, P.F., Birk, M., Boudon, V., Brown, L.R., Campargue, A., Champion, J.-P., Chance, K., Coudert, L.H., Dana, V., Devi, V.M., Fally, S., Flaud, J.-M., Gamache, R.R., Goldman, A., Jacquemart, D., Kleiner, I., Lacome, N., Lafferty, W.J., Mandin, J.-Y., Massie, S.T., Mikhailenko, S.N., Miller, C.E., Moazzen-Ahmadi, N., Naumenko, O.V., Nikitin, A.V., Orphal, J., Perevalov, V.I., Perrin, A., Predoi-Cross, A., Rinsland, C.P., Rotger, M., Šimečková, M., Smith, M.A.H., Sung, K., Tashkun, S.A., Tennyson, J., Toth, R.A., Vandaele, A.C., Vander Auwera, J., 2009. The HITRAN 2008 molecular spectroscopic database. J. Quant. Spectrosc. Radiat. Transf., HITRAN 110, 533–572. https://doi.org/10.1016/j.jqsrt.2009.02.013

Rothman, L.S., Jacquemart, D., Barbe, A., Chris Benner, D., Birk, M., Brown, L.R., Carleer, M.R., Chackerian Jr., C., Chance, K., Coudert, L.H., Dana, V., Devi, V.M., Flaud, J.-M., Gamache, R.R., Goldman, A., Hartmann, J.-M., Jucks, K.W., Maki, A.G., Mandin, J.-Y., Massie, S.T., Orphal, J., Perrin, A., Rinsland, C.P., Smith, M.A.H., Tennyson, J., Tolchenov, R.N., Toth, R.A., Vander Auwera, J., Varanasi, P., Wagner, G., 2005. The HITRAN 2004 molecular spectroscopic database. J. Quant. Spectrosc. Radiat. Transf. 96, 139–204. https://doi.org/10.1016/j.jqsrt.2004.10.008

Shannon, I., Harris, M., McHugh, D.R., Lewis, E.L., 1986. Low-pressure spectral line profiles: an analysis in terms of symmetric speed-dependent Voigt profiles. J. Phys. B At. Mol. Phys. 19, 1409. https://doi.org/10.1088/0022-3700/19/10/011

Smith, K.M., Newnham, D.A., 2000. Near-infrared absorption cross sections and integrated absorption intensities of molecular oxygen (O_2, O_2-O_2, and O_2-N_2). J. Geophys. Res. Atmospheres 105, 7383–7396. https://doi.org/10.1029/1999JD901171

Smith, K.M., Newnham, D.A., Williams, R.G., 2001. Collision-induced absorption of solar radiation in the atmosphere by molecular oxygen at 1.27 μm: Field observations and model calculations. J. Geophys. Res. Atmospheres 106, 7541–7552. https://doi.org/10.1029/2000JD900699

864 Strong, K., Mendonca, J., Weaver, D., Fogal, P., Drummond, J.R., Batchelor, R., Lindenmaier, R., 2017. TCCON
865   data from Eureka (CA), Release GGG2014.R1.
866   https://doi.org/10.14291/tccon.ggg2014.eureka01.R1/1325515
867 Toon, G. C., 2014a. Telluric line list for GGG2014, TCCON data archive. Carbon Dioxide Inf. Anal. Cent. Oak
868   Ridge Natl. Lab. Oak Ridge Tenn. USA. https://doi.org/10.14291/tccon.ggg2014.atm.R0/1221656
869 Toon, G. C., 2014b. Solar line list for GGG2014. TCCON Data Arch. Hosted Carbon Dioxide Inf. Anal. Cent. Oak
870   Ridge Natl. Lab. Oak Ridge Tenn. USA.
871 Toon, G.C., 1991. The JPL MkIV interferometer. Opt. Photonics News 2, 19–21.
872   https://doi.org/10.1364/OPN.2.10.000019
873 Tran, H., Boulet, C., Hartmann, J.-M., 2006. Line mixing and collision-induced absorption by oxygen in the A band:
874   Laboratory measurements, model, and tools for atmospheric spectra computations. J. Geophys. Res.
875   Atmospheres 111, D15210. https://doi.org/10.1029/2005JD006869
876 Tran, H., Hartmann, J.-M., 2008. An improved O_2 A band absorption model and its consequences for retrievals of
877   photon paths and surface pressures. J. Geophys. Res. Atmospheres 113, D18104.
878   https://doi.org/10.1029/2008JD010011
879 Tran, H., Ngo, N.H., Hartmann, J.-M., 2013. Efficient computation of some speed-dependent isolated line profiles.
880   J. Quant. Spectrosc. Radiat. Transf. 129, 199–203. https://doi.org/10.1016/j.jqsrt.2013.06.015
881 Wallace, L., Livingston, W., 1990. Spectroscopic observations of atmospheric trace gases over Kitt Peak. I - Carbon
882   dioxide and methane from 1979 to 1985. J. Geophys. Res. 95, 9823–9827.
883   https://doi.org/10.1029/JD095iD07p09823
884 Washenfelder, R.A., Toon, G.C., Blavier, J.-F., Yang, Z., Allen, N.T., Wennberg, P.O., Vay, S.A., Matross, D.M.,
885   Daube, B.C., 2006. Carbon dioxide column abundances at the Wisconsin Tall Tower site. J. Geophys. Res.
886   Atmospheres 111, D22305. https://doi.org/10.1029/2006JD007154
887 Wehr, R.A., 2005. Dicke -narrowed spectral lines in carbon monoxide buffered by argon (Ph.D.). University of
888   Toronto (Canada), Canada.
889 Wennberg, P.O., Roehl, C.M., Wunch, D., Toon, G.C., Blavier, J.-F., Washenfelder, R., Keppel-Aleks, G., Allen,
890   N.T., Ayers, J., 2017a. TCCON data from Park Falls (US), Release GGG2014.R0.
891   https://doi.org/10.14291/tccon.ggg2014.parkfalls01.R0/1149161
892 Wennberg, P.O., Wunch, D., Roehl, C.M., Blavier, J.-F., Toon, G.C., Allen, N.T., Dowell, P., Teske, K., Martin, C.,
893   Martin, J., 2017b. TCCON data from Lamont (US), Release GGG2014.R0.
894   https://doi.org/10.14291/tccon.ggg2014.lamont01.R0/1149159
895 Wójtewicz, S., Cygan, A., Masłowski, P., Domysławska, J., Lisak, D., Trawiński, R.S., Ciuryło, R., 2014. Spectral
896   line shapes of self-broadened P-branch transitions of oxygen B band. J. Quant. Spectrosc. Radiat. Transf.
897   144, 36–48. https://doi.org/10.1016/j.jqsrt.2014.03.029
898 Wunch, D., Toon, G.C., Blavier, J.-F.L., Washenfelder, R.A., Notholt, J., Connor, B.J., Griffith, D.W.T., Sherlock,
899   V., Wennberg, P.O., 2011. The Total Carbon Column Observing Network. Philos. Trans. R. Soc. Math.
900   Phys. Eng. Sci. 369, 2087–2112. https://doi.org/10.1098/rsta.2010.0240
901 Wunch, D., Toon, G.C., Sherlock, V., Deutscher, N.M., Liu, C., Feist, D.G., Wennberg, P.O., 2015. The Total
902   Carbon Column Observing Network's GGG2014 Data Version.
903   https://doi.org/10.14291/tccon.ggg2014.documentation.R0/ 1221662
904 Wunch, D., Toon, G.C., Wennberg, P.O., Wofsy, S.C., Stephens, B.B., Fischer, M.L., Uchino, O., Abshire, J.B.,
905   Bernath, P., Biraud, S.C., Blavier, J.-F.L., Boone, C., Bowman, K.P., Browell, E.V., Campos, T., Connor,
906   B.J., Daube, B.C., Deutscher, N.M., Diao, M., Elkins, J.W., Gerbig, C., Gottlieb, E., Griffith, D.W.T.,
907   Hurst, D.F., Jiménez, R., Keppel-Aleks, G., Kort, E.A., Macatangay, R., Machida, T., Matsueda, H.,
908   Moore, F., Morino, I., Park, S., Robinson, J., Roehl, C.M., Sawa, Y., Sherlock, V., Sweeney, C., Tanaka,
909   T., Zondlo, M.A., 2010. Calibration of the Total Carbon Column Observing Network using aircraft profile
910   data. Atmos Meas Tech 3, 1351–1362. https://doi.org/10.5194/amt-3-1351-2010
911 Yang, Z., Toon, G.C., Margolis, J.S., Wennberg, P.O., 2002. Atmospheric CO_2 retrieved from ground-based near IR
912   solar spectra. Geophys. Res. Lett. 29, 1339. https://doi.org/10.1029/2001GL014537
913 Yokota, T., Yoshida, Y., Eguchi, N., Ota, Y., Tanaka, T., Watanabe, H., Maksyutov, S., 2009. Global
914   Concentrations of CO_2 and CH_4 Retrieved from GOSAT: First Preliminary Results. Sola 5, 160–163.
915   https://doi.org/10.2151/sola.2009-041
916 Yu, S., Drouin, B.J., Miller, C.E., 2014. High resolution spectral analysis of oxygen. IV. Energy levels, partition
917   sums, band constants, RKR potentials, Franck-Condon factors involving the $X^3\Sigma_g^-$, $a^1\Delta_g$ and $b^1\Sigma_g^+$ states. J.
918   Chem. Phys. 141, 174302. https://doi.org/10.1063/1.4900510
919

920

921 **Figures**
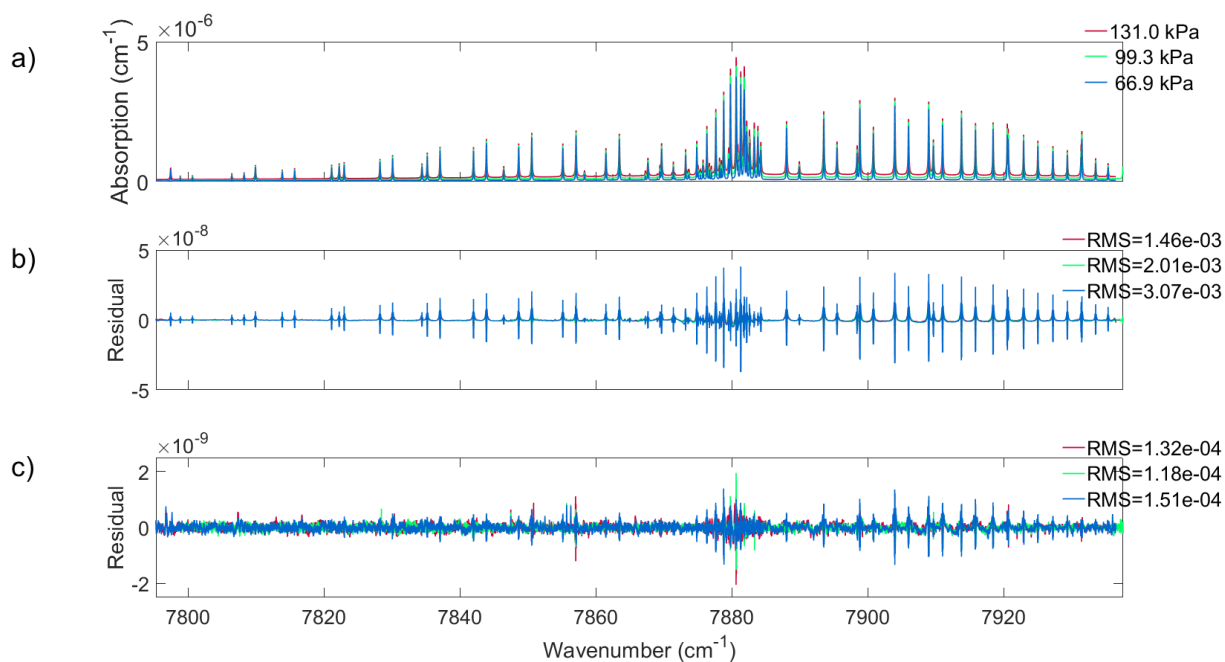
922

923 **Figure 1: (a) Cavity-ring-down absorption coefficients** <mark>**for O₂**</mark> **measured at** <mark>**the**</mark> **three pressures indicated in the**
924 **legend at approximately room temperature and a volume mixing ratio of 0.20720(43)** ~~**for O₂**~~**. The difference**
925 **between measured absorption coeffcients and those calculated using (b) a Voigt line shape**<mark>**,**</mark> **and (c) the speed-**
926 **dependent Voigt line shape. Note the difference in scale between panels (b) and (c).**

927

928

929
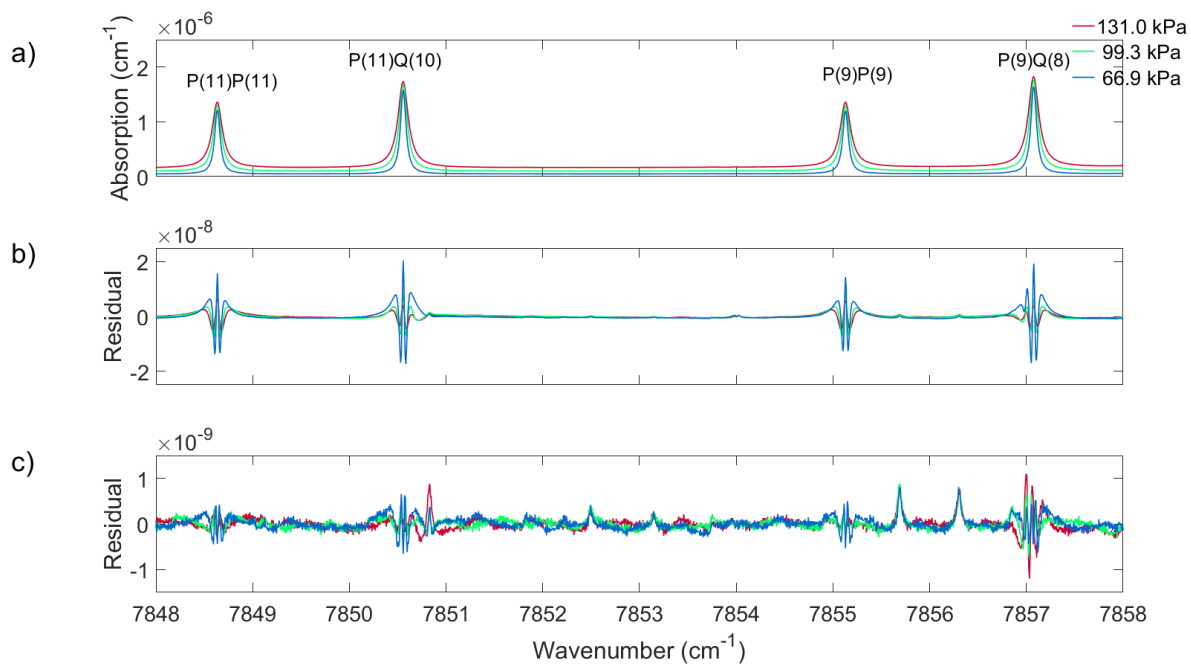
Figure 2: The same as Figure 1 but ~~zoomed into~~ **expanded to show** four spectral lines in the P branch of the O₂ 1.27 μm band.

940
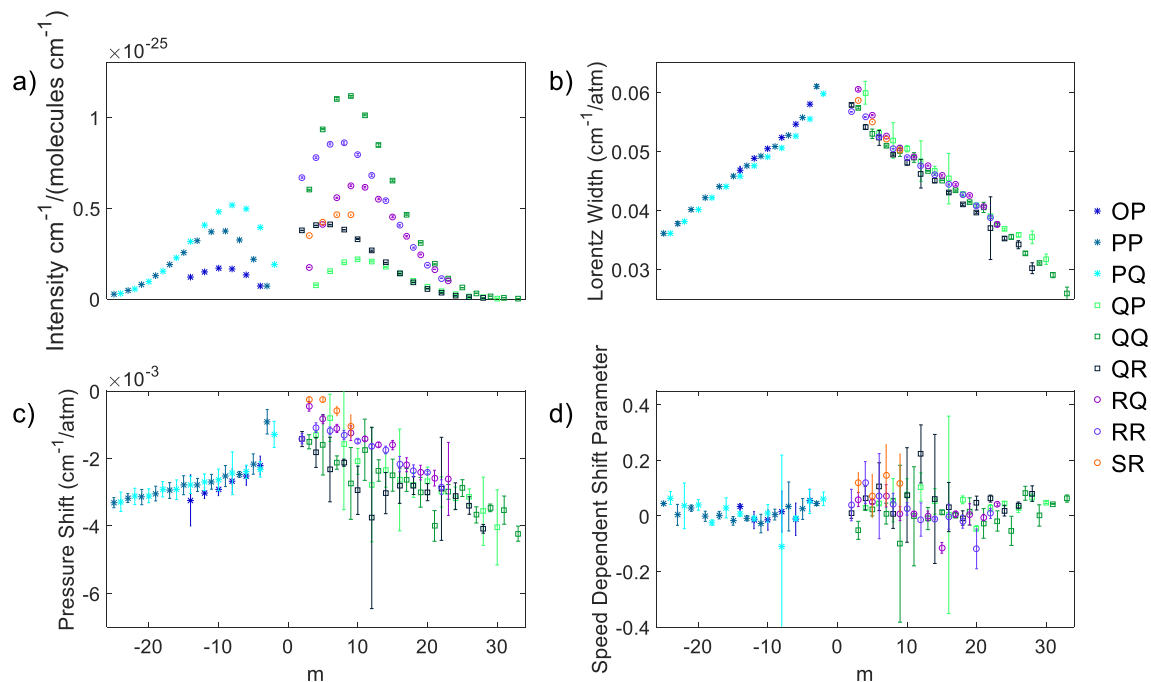
Figure 3: The averaged measured (a) intensity, (b) Lorentz line width, (c) pressure shift, and (d) speed-dependent pressure shift retrieved from the three cavity ring-down spectra of the 1.27 μm band of O_2. All data are plotted as a function of ~~lower state rotational quantum number J~~ m which is m =-J for the P-branch lines, m=J for the Q-branch, and m=J+1 for the R-branch (where J is the lower state rotational quantum number) and the uncertainties shown are 2σ.

946

947

948

949

950

951

952

953
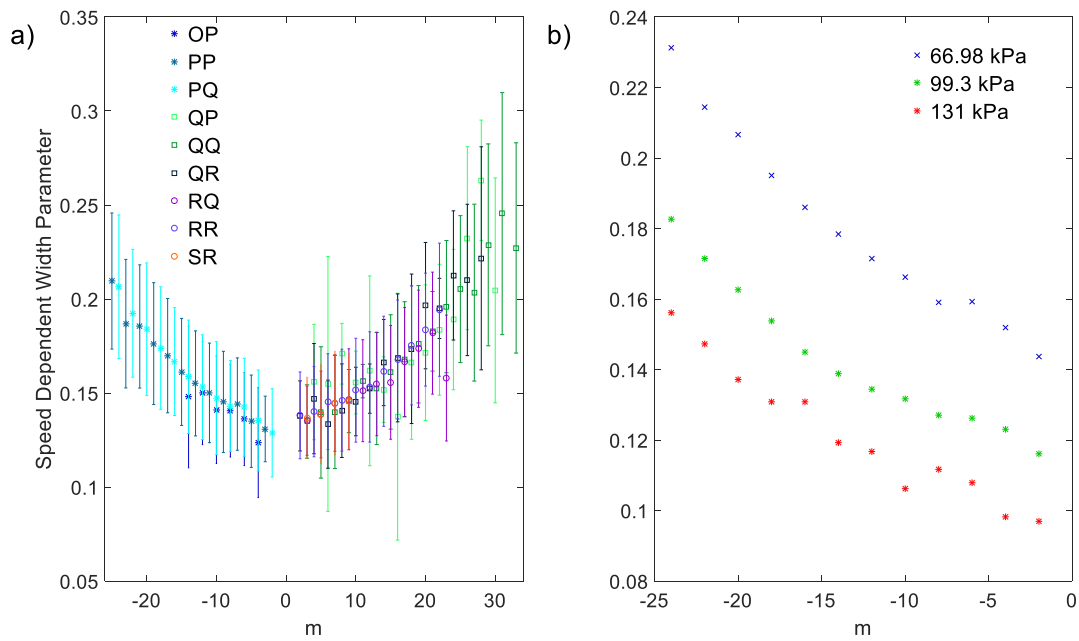
Figure 4: (a) The averaged measured speed-dependent width parameter of the 1.27 μm band of O$_2$ plotted as a function of m.~~lower state rotational quantum number *J″*.~~ (b) The measured speed-dependent width parameter for spectral lines that belong to the PQ sub-branch plotted as a function of m.~~lower state rotational quantum number *J″*.~~

958

959

960

961

962
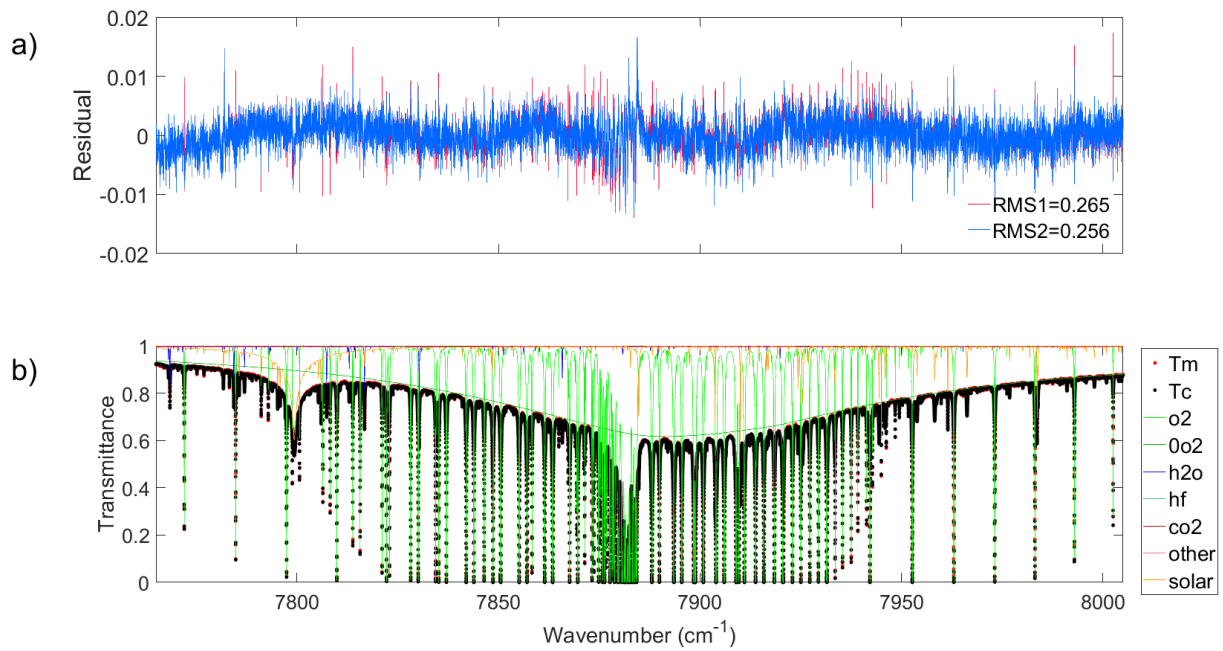
Figure 5: (a) The residuals (measured minus calculated) for a spectrum measured at Eureka on March 27, 2015 at a SZA of 81.32º. The red residual is the result of using the Voigt line shape and the blue is from using the qSDV. (b) The measured (red dots) and calculated (black dots), with the qSDV, spectrum, along with the gases included in the fit (refer to the legend to the right) in the spectral window.

967

968

969

970

971

972
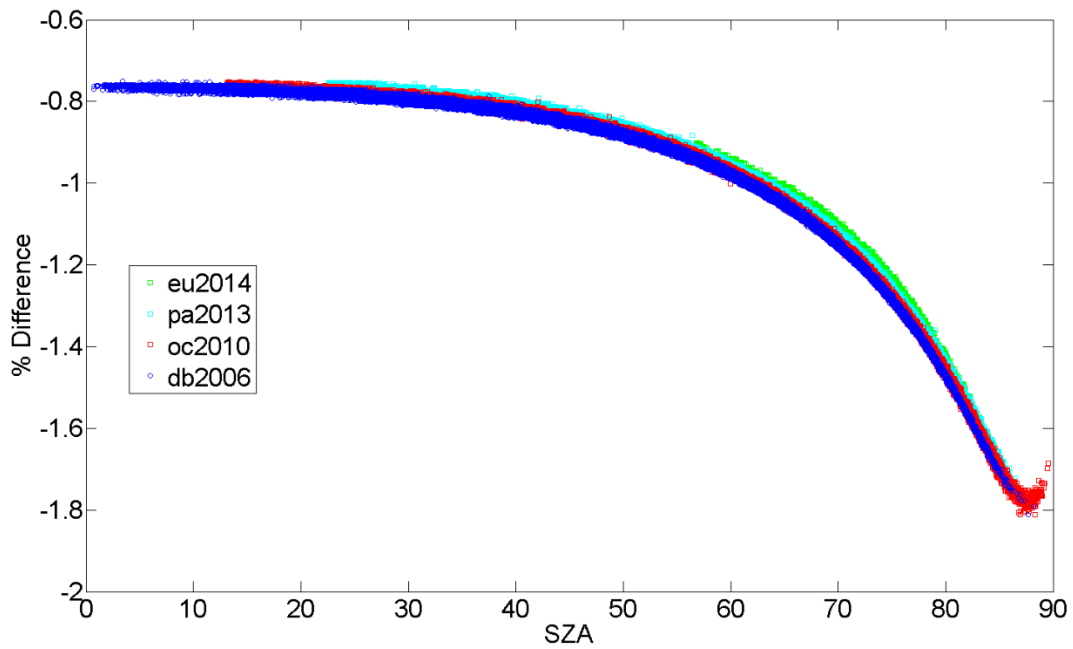
973

974 **Figure 6: The percent difference between the O_2 column retrieved with the Voigt and qSDV line shapes for a**
975 **year of measurements from Eureka (eu), Park Falls (pa), Lamont (oc), and Darwin (db).**

976

977

978

979

980
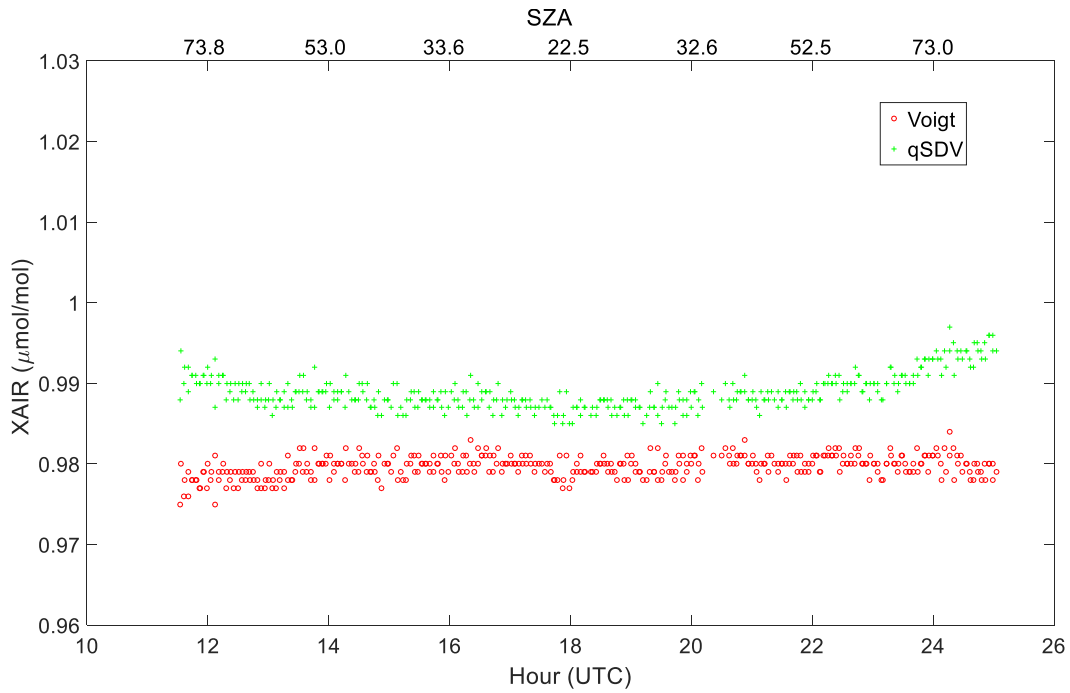
Figure 7: XAIR from Park Falls retrieved from spectra recorded on June 18, 2013. XAIR is calculated using O$_2$ columns retrieved using a Voigt (red) and qSDV (green) line shapes. The top x-axis is the SZA that corresponds to the hour on the bottom x-axis.

984

985

986

987

988
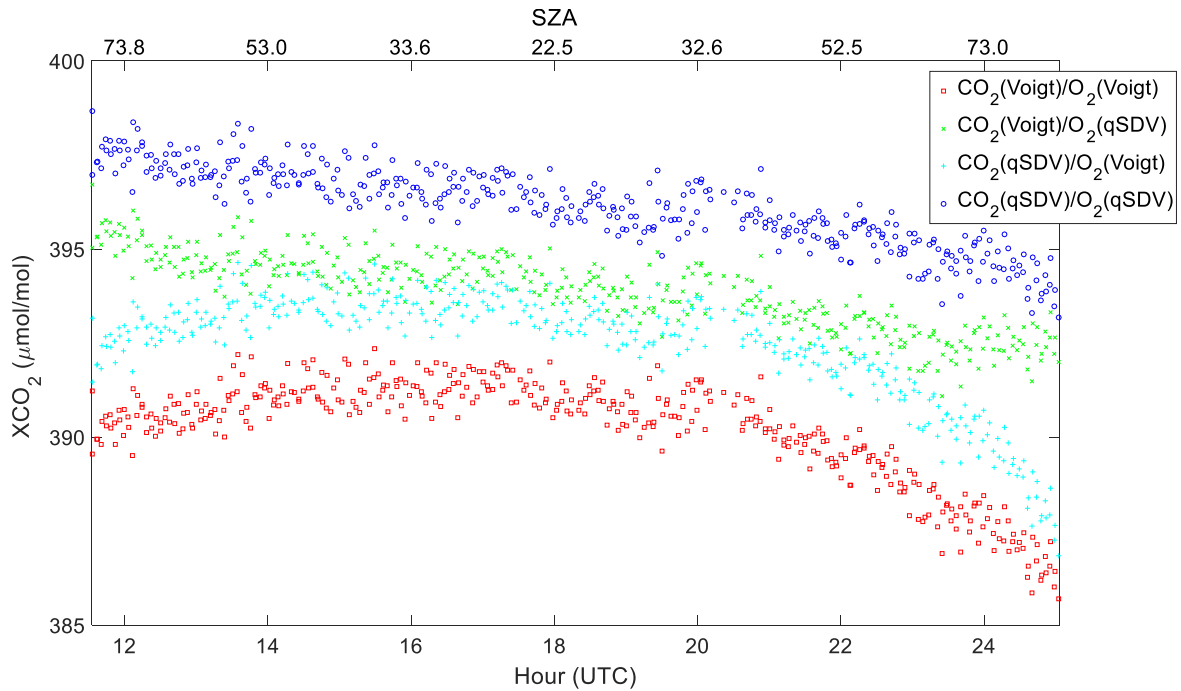
Figure 8: XCO₂ calculated from the CO₂ and O₂ columns retrieved from Park Falls spectra recorded on June 18, 2013. The CO₂ columns were retrievied using either the Voigt line shape or the qSDV with line mixing, while the O₂ columns were retrieved using either the Voigt or qSDV line shapes. XCO₂ was calculated in four ways: 1) Both CO₂ and O₂ columns retrieved using the Voigt line shape (red), 2) CO₂ columns retrieved with the Voigt and O₂ columns retrieved with the qSDV (green), 3) CO₂ columns retrieved with the qSDV and line mixing and O₂ columns retrieved with the Voigt (cyan), and 4) CO₂ columns retrieved with the qSDV and line mixing and O₂ columns retrieved with the qSDV (blue). The top x-axis is the SZA that corresponds to the hour on the bottom x-axis.

997

998
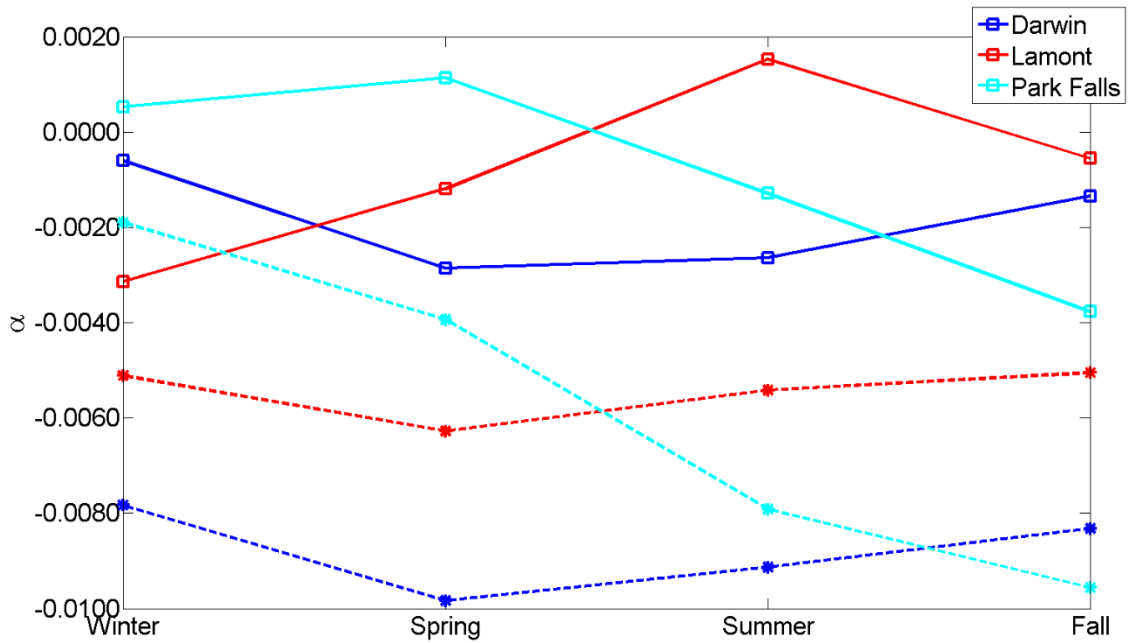
999

1000 **Figure 9~~7~~: The average airmass-dependent correction factor for XCO₂ derived from a year of spectra**
1001 **measured at Darwin, Lamont, and Park Falls for different seasons. The dashed lines with stars are the α for**
1002 **XCO₂ retrieved using a Voigt line shape for both CO₂ and O₂ columns. The solid lines with squares are from**
1003 **XCO₂ retrieved using the qSDV for both CO₂ and O₂ columns.**

1004

1005

1006

1007

1008

1009

1010
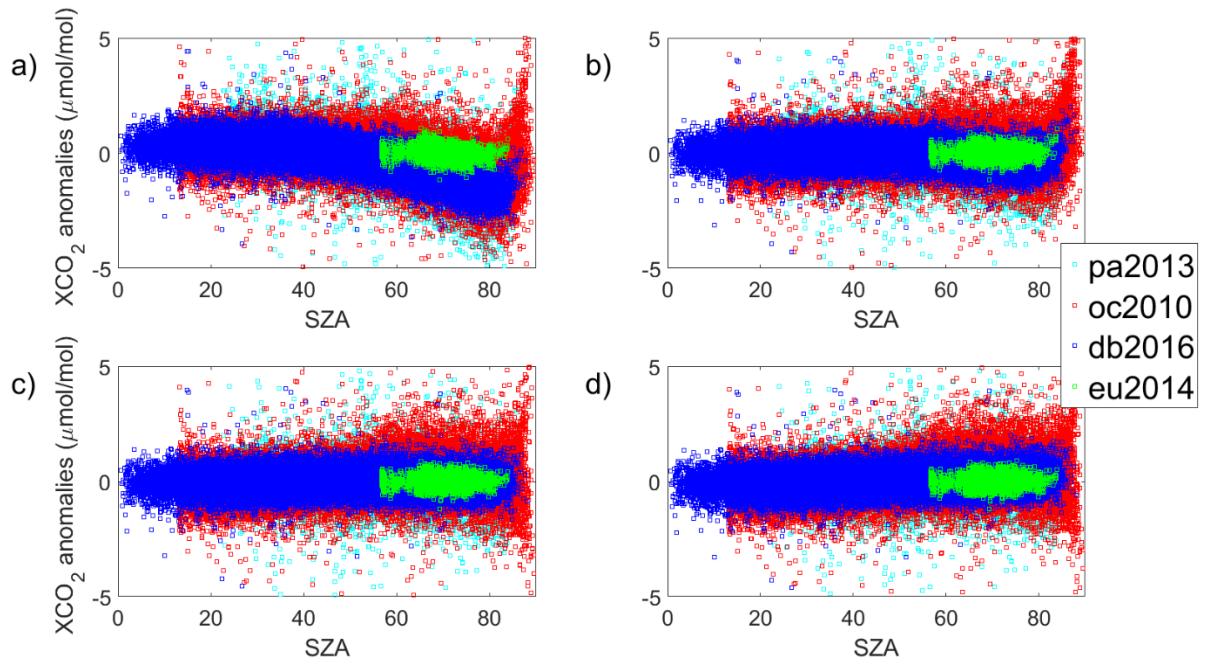
1011

1012   **Figure 10==8==: (a) XCO₂ Voigt anomaly for a year of measurements from the four TCCON sites. The XCO₂**
1013   **anomaly is the difference between each XCO₂ value and the daily median XCO₂. (b) The XCO₂ Voigt**
1014   **anomaly after the airmass dependence correction is applied to the XCO₂ Voigt data. (c) XCO₂ qSDV**
1015   **anomaly. (d) XCO₂ qSDV anomaly after correction for the airmass dependence.**

1016

1017

1018

1019

1020

1021
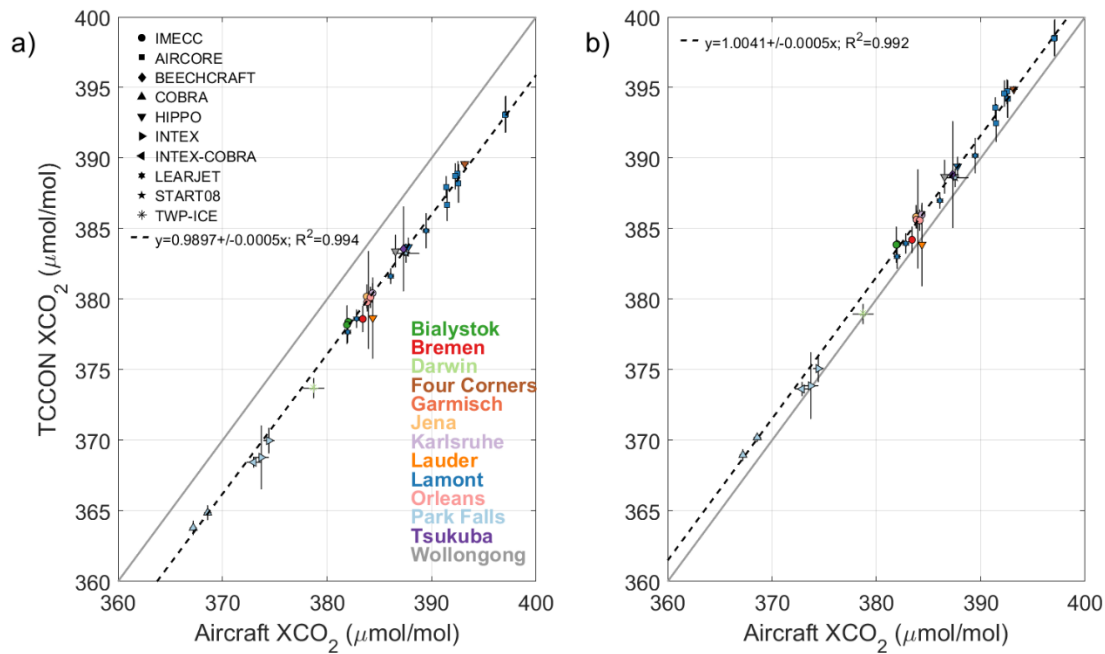
1022

**Figure 119: (a) Correlation between TCCON and aircraft XCO₂ Voigt measurements for 13 TCCON sites.
Each aircraft type is indicated by a different symbol given by the legend in the top left corner. Each site is
represented by a different colour given by the legend in the bottom right corner. The grey line indicates the
one-to-one line and the dashed line is the line of best fit for the data. The slope of the line of best fit as well as
the error on the slope are given in the plot. (b) the same as (a) but for XCO₂ qSDV.**

1023
1024
1025
1026
1027

1028

1029

1030
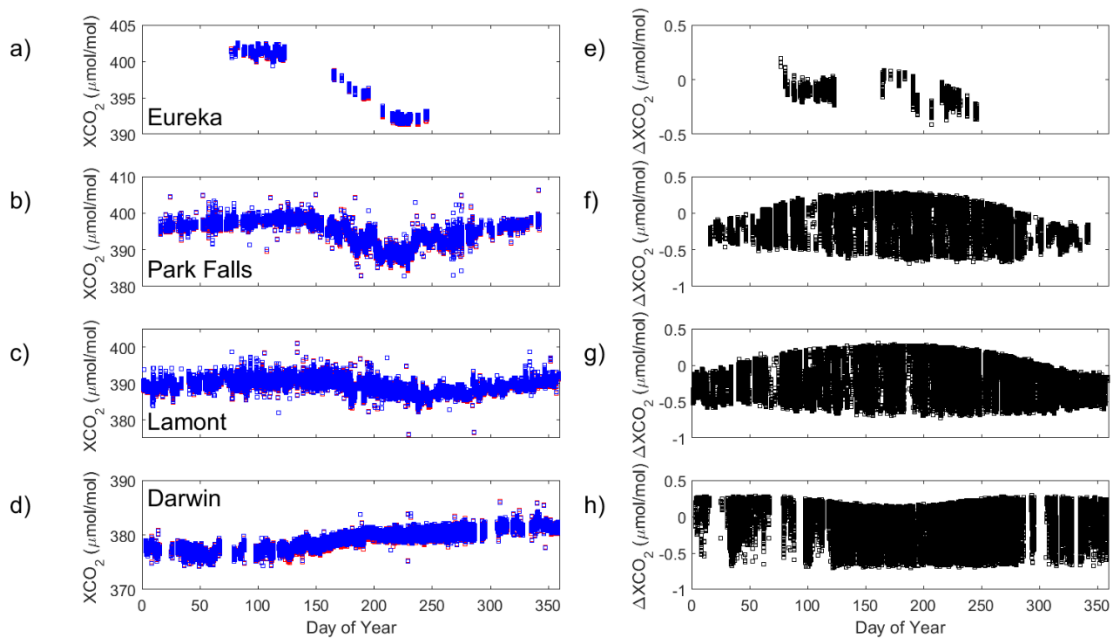
1031

1032   **Figure 12~~10~~: (a) to (d) XCO₂ plotted as a function of day of the year for Eureka (2014), Park Falls (2013),**
1033   **Lamont (2010), and Darwin (2006) respectively. The mostly-hidden red boxes are XCO₂ calculated from**
1034   **using a Voigt line shape in the retrieval and the blue boxes are from using the qSDV. (e) to (h) the difference**
1035   **between XCO₂ Voigt and XCO₂ qSDV.**

1036

1037

1038

1039
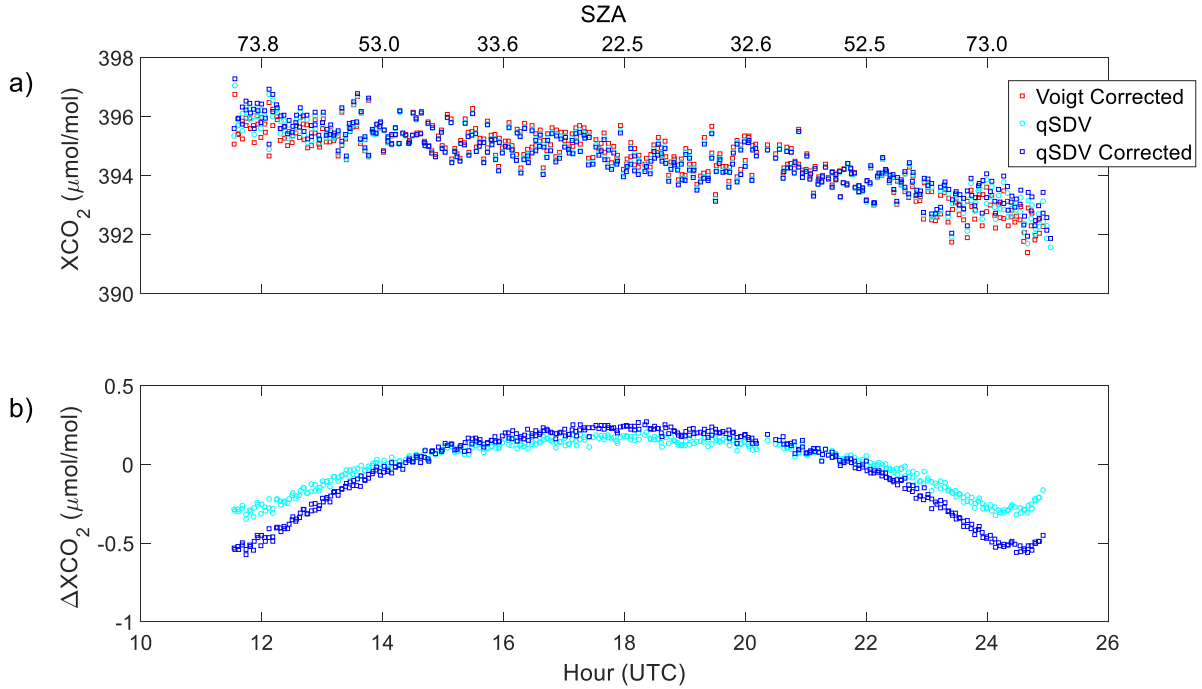
1040

Figure 13~~11~~: (a) XCO₂ from Park Falls retrieved from spectra recorded on June 18, 2013. Plotted is XCO₂ retrieved: (1) with a Voigt line shape and corrected for the airmass dependence (red squares), (2) with the qSDV (cyan circles), and (3) with the qSDV and corrected for the airmass dependence (blue squares). (b) the difference between the Voigt XCO₂ corrected and the qSDV XCO₂ (cyan circles), and the difference between the Voigt XCO₂ corrected and the qSDV XCO₂ corrected (blue squares). The top x-axis is the SZA that corresponds to the hour on the bottom x-axis.

1041
1042
1043
1044
1045
1046

1047